Contrib Mineral Petrol (2013) 165:349–372
DOI 10.1007/s00410-012-0812-y

ORIGINAL PAPER

Timescales of crustal melting in the Higher Himalayan Crystallines (Sikkim, Eastern Himalaya) inferred from trace element-constrained monazite and zircon chronology

Daniela Rubatto · Sumit Chakraborty · Somnath Dasgupta

Received: 15 June 2012 / Accepted: 8 September 2012 / Published online: 28 September 2012

Abstract The petrology and timing of crustal melting has been investigated in the migmatites of the Higher Himalayan Crystalline (HHC) exposed in Sikkim, India. The metapelites underwent pervasive partial melting through hydrous as well as dehydration melting reactions involving muscovite and biotite to produce a main assemblage of quartz, K-feldspar, plagioclase, biotite, garnet ± sillimanite. Peak metamorphic conditions were 8–9 kbar and ~800 °C. Monazite and zircon crystals in several migmatites collected along a N–S transect show multiple growth domains. The domains were analyzed by microbeam techniques for age (SHRIMP) and trace element composition (LA-ICP-MS) to relate ages to conditions of formation. Monazite preserves the best record of metamorphism with domains that have different zoning pattern, composition and age. Zircon was generally less reactive than monazite, with metamorphic growth zones preserved in only a few samples. The growth of accessory minerals in the presence of melt was episodic in the interval between 31 and 17 Ma, but widespread and diachronous across samples. Systematic variations in the chemical composition of the dated mineral zones (HREE content and negative Eu anomaly) are related to the variation in garnet and K-feldspar abundances, respectively, and thus to metamorphic reactions and P–T stages. In turn, this allows prograde versus decompressional and retrograde melt production to be timed. A hierarchy of timescales characterizes melting which occurred over a period of ~15 Ma (31–17 Ma): a given block within this region traversed the field of melting in 5–7 Ma, whereas individual melting reactions lasted for time durations below, or approaching, the resolution of microbeam dating techniques (~0.6 Ma). An older ~36 Ma high-grade event is recorded in an allocthonous relict related to mafic lenses. We identify two sections of the HHC in Sikkim that traversed similar P–T conditions at different times, separated by a tectonic discontinuity. The higher structural levels reached melting and peak conditions later (~26–23 Ma) than the lower structural levels (~31–27 Ma). Diachronicity across the HHC cannot be reconciled with channel flow models in their simplest form, as it requires two similar high-grade sections to move independently during collision.

Keywords U–Pb geochronology · Migmatites · Trace elements · Himalaya · Melting reactions

Communicated by J. Hoefs.

Electronic supplementary material The online version of this article (doi:10.1007/s00410-012-0812-y) contains supplementary material, which is available to authorized users.

D. Rubatto (✉)
Research School of Earth Sciences, Australian National University, Canberra 0200, Australia
e-mail: Daniela.rubatto@anu.edu.au

S. Chakraborty
Institut fuer Geologie, Mineralogie und Geophysik, Ruhr-Universität Bochum, 44780 Bochum, Germany

S. Dasgupta
Department of Earth Sciences, Indian Institute of Science Education and Research, Salt Lake, Kolkata 700064, India

Introduction

The dynamics of crustal melting (timing, duration and productivity) in collisional settings has major implications for the evolution of the overriding orogen. It has, for example, the capacity to change the rheology of the thickened crust and trigger exhumation (e.g., Faccenda

et al. 2008). Melting in felsic rocks and metapelites, as commonly found in mountain belts, occurs by a variety of reactions that occur with increasing temperature—from fluid-induced melting to muscovite dehydration melting and biotite dehydration melting (Spear et al. 1999; White et al. 2003; Dasgupta et al. 2009). The productivity of the melting process (amount of melt produced over time per unit mass of rock) depends on which melting reactions are reached during the P–T–time evolution, the availability of fluids and the bulk rock composition. The latter can be reasonably estimated from the observed composition. The P–T evolution of migmatites can be established using conventional thermobarometry and thermodynamic modeling (e.g., White et al. 2003; Harris et al. 2004; Dasgupta et al. 2009).

Determining the time that a rock unit spends in the melting field is not trivial. For this, the stage (during P–T evolution) at which datable minerals crystallized needs to be identified by a combination of thermodynamic modeling, study of structural and microtextural controls, and interpretation of microchemical indicators. Successful studies have used U–Pb dating of accessory minerals that crystallized from the melts at different points along the P–T path (Oliver et al. 1999; Rubatto et al. 2001; Williams 2001; Hermann and Rubatto 2003; Viskupic et al. 2005; Rubatto et al. 2009; Liu et al. 2010; Imayama et al. 2012). In sub-solidus metamorphic environments, accessory minerals either recrystallize or form as a result of solid-state reactions, for example through reactions between allanite and monazite (see Spear and Pyle 2002; Janots et al. 2008; Spear 2010). In melt-present conditions, the undersaturation/saturation of the melt in specific components controls dissolution or precipitation of accessory minerals such as zircon and monazite. The details of such dissolution/precipitation may depend on many factors in addition to intensive thermodynamic variables (e.g., P, T, f_{H_2O}), such as the abundance and local distribution of melts. The latter can depend in turn on processes such as deformation. Given that multiple melting and crystallization reactions occur during the P–T evolution of a rock, all of these factors evolve continually and may result in multiple episodes of dissolution/precipitation during a single P–T cycle. Consideration of the stratigraphy of zoning and cross-cutting relations within an accessory mineral grain allows a relative sequence of events to be constructed; consideration of trace element signatures in these zones may allow the formation of a zone to be related to variation in modal abundances of major mineral phases. The latter, in turn, is connected to metamorphic reactions (Foster et al. 2000; Pyle and Spear 2003; Rubatto et al. 2006). Therefore, simultaneous consideration of zoning, trace element distribution and isotopic dating may allow different stages in the P–T evolution of a rock to be delineated.

The Higher Himalayan Crystallines (HHC) provide an excellent natural laboratory for studying the course of melting in pelitic rocks during orogenesis because all observations of Himalayan age can be attributed to a single, known orogenic process—the ongoing collision of India with Asia. The rocks are recent and no overprinting by a later orogenic event has occurred. The HHC is a thick sequence of high-grade rocks that crops out along the entire Himalayan chain and has traditionally been mapped as one unit, although local regional divisions have been discussed along various transects. Here, we present a detailed study of zircon and monazites from the HHC, which exposes large areas of migmatites. The geochronology of accessory minerals aims to investigate the timing of melting, and more specifically of melting reactions, and the presence of any regional diachronism or synchronicity in melting across a ~40-km section exposed in Sikkim (NE India).

Monazite has been the preferred chronometer for Himalayan metamorphic rocks given (i) the reactivity of monazite during Barrovian metamorphism, even at medium grade and in sub-solidus conditions, (ii) the abundance of monazite in most Himalayan metapelites and, of course, (iii) the robustness of the U–Pb system at high temperatures. Monazite has often been dated in its textural context (e.g., Harrison et al. 1997; Catlos et al. 2002; Catlos et al. 2004; Kohn et al. 2005; Martin et al. 2007), and the composition and internal zoning of monazite has been utilized to interpret the ages (Foster et al. 2000; Kohn et al. 2005; Viskupic et al. 2005; Carosi et al. 2010; Kellett et al. 2010). However, the robustness of monazite ages and their interpretation in terms of metamorphic conditions remain disputed in many cases (Kohn et al. 2005; Martin et al. 2007).

The use of zircon geochronology in addressing Himalayan metamorphism is scarce (Imayama et al. 2012) and is generally limited to granites and melt mobilisates (Viskupic et al. 2005; Cottle et al. 2009b). The limited formation of metamorphic zircon during sub-solidus metamorphism (Rubatto et al. 2001) is one reason for the paucity of zircon geochronology. In partially molten rocks, however, the combination of zircon and monazite geochronology can deliver complementary information, as has been shown in case studies (Rubatto et al. 2001; Rubatto et al. 2006) or predicted by modeling (Kelsey et al. 2008).

The area of Sikkim where we investigate the HHC exposes a spectacular variety of migmatites for which metamorphic evolution and melting reactions are reasonably well known, but geochronology is practically absent. In this study, we have linked the U–Pb ages obtained from specific growth zones of zircon and monazite to melting reactions predicted by thermodynamic grids or pseudosections using microtextures and variations in the trace

element composition of the dated minerals. The information obtained from the two accessory minerals from nine samples within a single section allows us to relate ages to melting reactions and coexisting assemblages and evaluate whether the section is continuous. In addition, issues of tectonic and regional significance are also addressed through such a study. For example: Is the distribution of ages homogenous across the HHC belt in an area, or are there patterns of age distribution? How long did melting last, and what was the chronological evolution (i.e., timing and duration) of melting across the belt? Answers to these questions are necessary in order to address the larger tectonic issues such as whether melting may have provided enough buoyancy to trigger exhumation, what the extent of compression/convergence was, and if channel flow (Jamieson et al. 2004), or other kinds of tectonic processes were (are!) operative.

Geology of the Sikkim region

The Himalaya is a 2,500-km-long orogenic zone (inset in Fig. 1) resulting from the collision of India with Eurasia beginning at about 55 Ma. The Sikkim region in eastern Himalaya exposes a complete section of the Himalayan edifice, from the sediments of the foreland to the Tethyan sequence (Fig. 1). The main tectonic boundaries and geological units within this section are from south to north: 1) the Main Boundary Thrust that juxtaposes the Mio-Pliocene molasses of the Siwalik Group with the lesser Himalayan (LH) belt, which exposes a window of low-grade sediments of the Gondwana Group within the thick metasedimentary package of the Daling Group; 2) the Main Central Thrust (MCT) marks the boundary between the "inverted metamorphic sequence" of the LH with the high-grade rocks and migmatites of the HHC; 3) in the far north, the HHC is truncated by a series of north-dipping normal faults constituting the South Tibetan Detachment (STDS). At the hanging wall of this detachment are the fossiliferous sediments of the Tibetan sequence.

The lesser Himalayan sequence preserves a complete inverted Barrovian zone from chlorite to sillimanite—K-feldspar grade, where higher metamorphic grades lie successively at higher structural levels from south to north (Fig. 1; Dasgupta et al. 2004; Dasgupta et al. 2009). Muscovite is completely eliminated in the sillimanite—K-feldspar zone. Maximum P–T conditions recorded at the top of the LH sequence are ~7.5 kbar, 700 °C (Dasgupta et al. 2004). Melt production in the LH metapelites is ascribed to a series of melting reactions with increasing temperature (Dasgupta et al. 2009), starting from paragonite melting in the kyanite-zone (mineral abbreviations according to Kretz 1983)

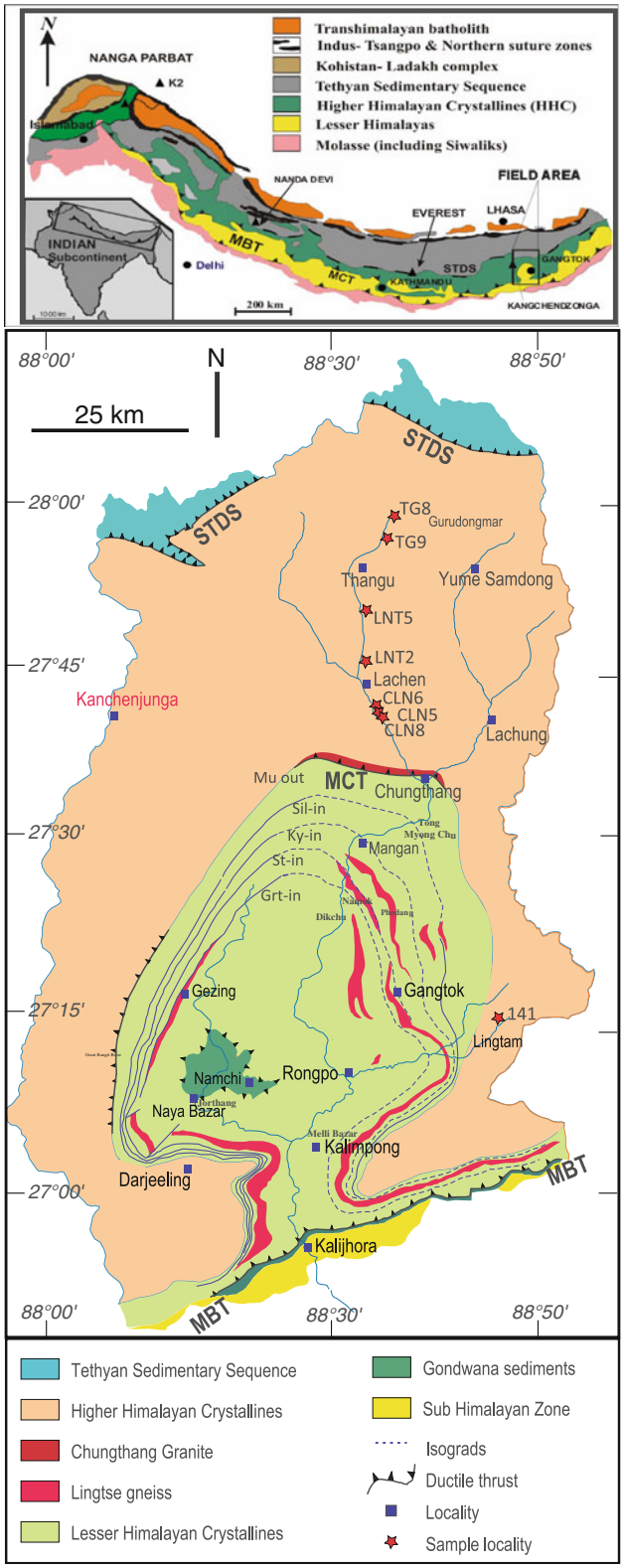

Fig. 1 **a** An overview of the major lithological and structural units of Himalaya and location of the study area. **b** Geological map of Sikkim Himalaya with sample location, compiled and modified by Mukhopadhyay and others (in preparation) after Ghosh (1956), Acharryya and Ray (1977), Lal et al. (1981) and Ray (2000). *MBT* main boundary thrust, *MCT* main central thrust, *STDS* South Tibetan detachment system

$$Pg + Ab + Qtz + H_2O = melt \pm Grt \quad (1)$$

to dehydration melting of muscovite

$$Ms + Qtz \pm Pl = Grt + Sil \pm Kfs + melt \quad (2)$$

and, finally to dehydration melting of biotite

$$Bt + Sil + Qtz + Pl = Grt \pm Kfs + melt \quad (3)$$

The LH sequence is separated from the HHC by the Main Central Thrust just north of Chungthang (Fig. 1), which also coincides with the occurrence of an orthogneiss of granitic composition (Chungthang Granite in Fig. 1).

The present investigation is concerned with the migmatites of the HHC, which are dominated by metapelitic rocks. These are intercalated with minor quartzites and calc-silicates, and with small bodies of mafic rocks (Faak et al. 2012) and orthogneisses. Metapelitic migmatites are in the biotite-melting interval with continued stability of the mineral along with sillimanite, K-feldspar, plagioclase, quartz, garnet, ilmenite, rutile, zircon, monazite, and locally, cordierite and spinel. There is no apparent P–T gradient in the sequence with peak P–T conditions reaching $\sim$10 kbar, 800 °C (Ganguly et al. 2000; Sorcar et al. in preparation). The migmatites evolved through a two-stage retrogression: an initial steep decompression to $\sim$5 kbar was followed by cooling down to 600 °C with little change in pressure. The retrograde P–T trajectory has been constrained with the help of both phase equilibria considerations and diffusional modeling of compositional zoning in garnet (Ganguly et al. 2000; Sorcar et al. in preparation).

Samples

Eight samples of metapelitic migmatites were collected along a N–S transect in north Sikkim, from Chungthang in the south to somewhat North of Thangu, close to the India-China border, in the north (Fig. 1; Table 1). Sample names refer to three segments of the transect: Chungthang to Lachen (CLN), Lachen to Thangu (LNT) and north of Thangu (TG). An additional sample (141/01) is from East Sikkim from a location to the east of Lingtam.

All the samples have clear migmatitic structure (Supplementary Fig. 1), generally with layers or pods of leucosome (quartzo-feldspatic portion representing former melt) at the cm-scale, interbanded with mesosome portions. In most outcrops, different generations of leucosome from layer-parallel to cross cutting are present. Some samples are particularly rich in leucosome (LNT5B and LNT2A), and one sample represents a segregated dm-thick leucosome (TG9A). All the samples along the N–S transect are derived from metapelites, as indicated by their Al-rich composition (sillimanite and garnet bearing) and detrital zircon population. Notably, metapelite LNT5B is directly

Table 1 Sample location and mineral assemblages

Label	Locality	GPS coordinates	Rock type	Main minerals	Minor	Retrogression
CLN5B	N–S transect, Chungthang-Lachen	27° 42.560 88° 33.561	Migmatitic metapelite	Qtz. Pl, Kfs, Bt, Grt, Sil	Ap, Mus	Spl + Qtz corona, Mus, green Bt, Chl
CLN6D	N–S transect, Chungthang-Lachen	27° 42.247 88° 33.727	Migmatitic metapelite	Qtz. Pl, Kfs, Bt, Grt, Sil	Ap, Ilm	Chl, sericite
CLN8A	N–S transect, Chungthang-Lachen	27° 40.957 88° 35.286	Migmatitic metapelite	Qtz. Pl, Kfs, Bt, Grt, Sil	Ap, Ilm	
LNT2A	N–S transect, Lachen-Thangu	27° 45.966 88° 32.550	Migmatitic metapelite rich in leucosome	Qtz. Pl, Kfs, Bt, Grt	Ap, Ilm	Crd + Bt symplectite, Chl, Mus, sericite, Bt
LNT5B	N–S transect, Lachen-Thangu	27° 50.266 88° 33.042	Migmatitic metapelite rich in leucosome	Qtz. Pl, Kfs, Bt, Grt	Ap, Ilm	green Bt, sericite
TG8C	N–S transect, Thangu	27° 58.702 88° 35.120	Migmatitic metapelite	Qtz. Pl, Kfs, Bt, Grt, Sil	Ky	Spl + Qtz symplectite
TG9C	N–S transect, Thangu	27° 57.093 88° 34.424	Migmatitic metapelite	Qtz. Pl, Kfs, Bt, Grt, Sil	Ilm	Spl + Qtz symplectite
TG9A	N–S transect, Thangu	27° 57.093 88° 34.424	Leucosome	Qtz. Pl, Kfs, Bt, Grt, Sil	Ky, Ap, Ilm	Spl + Qtz symplectite
141/01	SE Sikkim, Rangpo-Lingtam	27° 14.501 88° 46.031	Migmatitic orthogneiss	Qtz. Pl, Kfs, Bt, Grt, Sil	Ap	green Bt

Mineral abbreviations according to Kretz (1983)

in contact with an amphibolite pod that records different metamorphic conditions (9–12 kbar and 800 °C) than the metapelitic sequence (Faak et al. 2012).

Sample 141/01 from the east has a more felsic composition. Quartz and feldspars make up more than 70 % of the rock and garnet is rare. The inherited zircon population in this sample is peculiar in that it yields a single age group suggesting a magmatic protolith. Therefore, this sample is referred to as a migmatitic orthogneiss.

The samples investigated preserve a fresh HT assemblage comprising of quartz, K-feldspar, plagioclase, biotite, garnet ± sillimanite in variable proportions (Table 1; Fig. 2). *Garnet* varies in abundance from being dominating in the mesosome (CLN5B, CLN6D, CLN8A, LNT2A, TG8C and TG9C) to rare in more leucocratic samples (141/01, LNT5B and TG9A). Garnet crystals are rarely euhedral, and they either display low temperature retrogression (e.g., chlorite replacement along fractures, Fig. 2d) or, more commonly, replacement by sillimanite and biotite ± plagioclase and quartz (Fig. 2a, c, e), This replacement texture represents the reverse of reaction (3) above and occurred at high temperatures in the melt field. In a few samples (LNT5A and 141/01), garnet commonly occurs as skeletal or rounded grains associated with quartz and feldspars (Fig. 2b), which suggest its formation as a peritectic phase during melting [reaction (3) above].

Sillimanite is present in all but two samples (LNT2A and LNT5B), as fibrolite and/or as prismatic crystals (Fig. 2a, e, f). *Kyanite* is present as relict in the northernmost samples (TG8C and TG9A), which also contain abundant prismatic sillimanite (Fig. 2e). Kyanite is interpreted as a relict formed during the prograde path (<700 °C) before anatexis. In sample CLN5B, rare *white mica* laths occur that are distinct from the retrograde fine-grained mica and sericite that formed during retrogression (Fig. 2d). *Apatite and ilmenite* are minor (<5 % in volume) components of most samples.

Cordierite + biotite (LNT2A) or, in the TG samples, *spinel* + plagioclase symplectites (Fig. 2g) are found associated with garnet. Both of these indicate decompression at relatively high temperatures (Sorcar et al. in preparation). Other retrograde, low temperature minerals are green biotite, chlorite and fine-grained muscovite or sericite. Low T retrogression is particularly strong in the LNT samples (Fig. 2d), whereas it is minimal in the other samples.

Methods

Zircon and monazite crystals were separated after rock crushing using conventional heavy liquid and magnetic properties. The grains were mounted in epoxy resin and polished down to expose the near equatorial section. Cathodoluminescence (CL) on zircons was performed with a HITACHI S2250N scanning electron microscope supplied with an ellipsoidal mirror for CL. Operating conditions for the SEM were 15-kV, 60-μA and 20-mm working distance. Monazite back scattered images were produced with a Cambridge S360 scanning electron microscope working at 15 kV, ~2nA and a working distance of ~17 mm.

Trace element analyses of zircon and monazite were performed on the grain mount with a Laser Ablation—ICP-MS at ANU, using a pulsed 193-nm ArF Excimer laser with 100 mJ energy at a repetition rate of 5 Hz (Eggins et al. 1998) coupled to an Agilent 7500 quadrupole ICP-MS. External calibration was performed relative to NIST 612 glass, and internal standardization was based on stoichiometry of SiO_2 for zircon (32.45 wt%) and Ce for monazite (23.6 wt%). Accuracy and precision of the analyses were evaluated with a BCR-2G secondary glass standard and are always better than 10 % combined. Most LA-ICPMS analyses were performed on the 2-μm-deep U–Pb SHRIMP pit.

U, Th and Pb analyses were obtained with the sensitive high-resolution ion microprobes (SHRIMP II and SHRIMP RG) at ANU. Instrumental conditions and data acquisition were generally described by Williams (1998). The data were collected in sets of six scans throughout the masses, and a reference material was analyzed as every fourth analysis. For zircon, the measured $^{206}Pb/^{238}U$ ratio was corrected using reference zircon from the Temora granodiorite (417 Ma, Black et al. 2003), whereas for monazite, the adopted standard was Delaware 44069 (425 Ma, Aleinikoff et al. 2006). U–Pb data were collected over numerous sessions using the same standard, with the different analytical sessions having calibration errors between 1.4 and 2.7 % (2 sigma), which was propagated to single analyses. The analyses were corrected for common Pb based on the measured $^{207}Pb/^{206}Pb$ and assuming concordance, as described in Williams (1998). Reported ages are always $^{206}Pb/^{238}U$ unless otherwise indicated. The common Pb composition was assumed to be that predicted by the Stacey and Kramers (1975) model. It must be noted that the small percent of common Pb present in the analyses used for average age calculations (always <5 or 2 %, most commonly <1 or 0.5 % in zircon and monazite, respectively) ensures that any variation in Pb composition would not affect the results within the uncertainty given. Data evaluation and age calculation were done using the software Squid 1 and Isoplot/Ex (Ludwig 2003), respectively.

Average $^{206}Pb/^{238}U$ ages are quoted at 95 % confidence level (c.l.). We concentrate our interpretation on average age of statistically consistent populations of analyses. Little significance is attached to isolated or scattered ages that, in such complex samples, can result from analytical mixing between different domains despite the caution used in

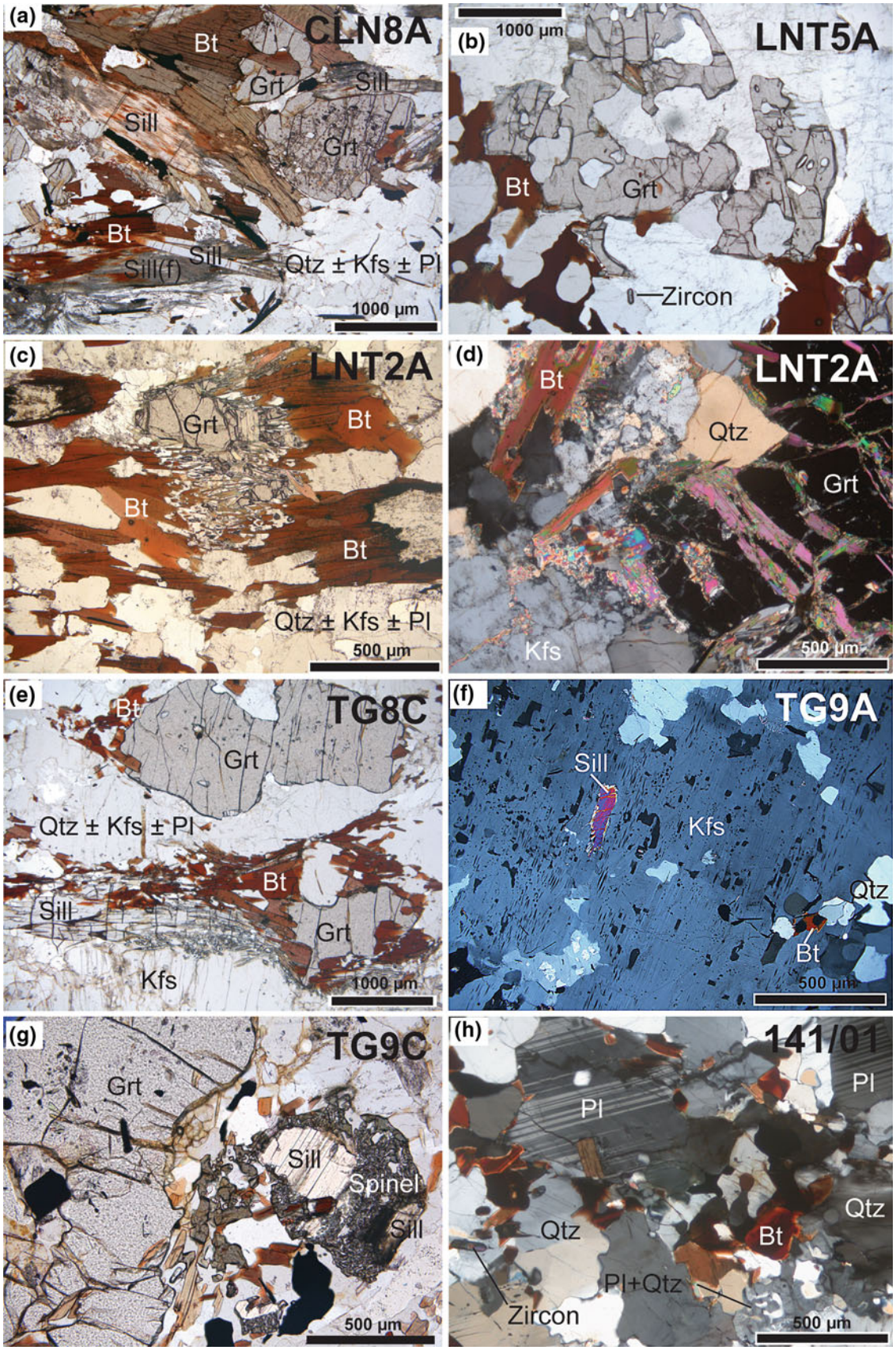
(a)
CLN8A
Bt
Grt
Sill
Sill
Grt
Bt
Sill
Sill(f)
Qtz ± Kfs ± Pl
1000 µm
(b)
1000 µm
LNT5A
Bt
Grt
Zircon
(c)
LNT2A
Grt
Bt
Bt
Bt
Qtz ± Kfs ± Pl
500 µm
(d)
Bt
LNT2A
Qtz
Grt
Kfs
500 µm
(e)
Bt
TG8C
Grt
Qtz ± Kfs ± Pl
Bt
Sill
Grt
Kfs
1000 µm
(f)
TG9A
Sill
Kfs
Qtz
Bt
500 µm
(g)
TG9C
Grt
Sill
Spinel
Sill
500 µm
(h)
141/01
Pl
Pl
Qtz
Qtz
Bt
Pl+Qtz
Zircon
500 µm

◀ **Fig. 2** Photomicrographs of thin sections of investigated samples. **a** Typical HT assemblage with fibrolite and prismatic sillimanite. **b** Skeletrical garnet indicating peritectic growth during melting. **c** Replacement of garnet by biotite + sillimanite + quartz ± plagioclase during retrogression. **d** Typical hydrous retrogression in LNT samples with abundant white mica and sericite and/or chlorite replacing garnet, biotite and K-feldspar. Crossed polarizer. **e** Replacement of garnet by biotite + sillimanite during retrogression. **f** Large K-feldspar in leucosome TG9A with relicts of sillimanite and biotite according to melting reaction (3). Crossed polarizer. **g** Spinel and plagioclase replacing sillimanite. **h** Large plagioclase crystals with twinning and wormy intergrowth of quartz and plagioclase in migmatitic orthogneiss 141/01. Note the large euhedral zircon. Crossed polarizer

identifying growth zones on the basis of CL and BSE images and in spite of the small penetration of the ion beam (~2 microns).

In leucosome TG9A, the analyzed zircon rims have high U contents (2,200–5,200 ppm) that correlated with the calculated $^{206}Pb/^{238}U$ age. This confirms the presence of a matrix effect that has been observed to affect SHRIMP zircon analyses with >2,500 ppm U (Butera et al. 2004; Hermann et al. 2006). For this sample, an age correction was made based on the linear regression between age and U ppm (slope of 0.00066). This amounts to a correction of ~−3 % for each 1,000 ppm of U above 2,500 ppm, which is comparable to what has been reported in other cases (Butera et al. 2004; Hermann et al. 2006).

For monazite analysis, energy filtering was applied (Rubatto et al. 2001) in order to eliminate the interference on ^{204}Pb and reduce the high counts on the ThO peak. Energy filtering is also expected to reduce any matrix effect, and indeed, a correlation between isotopic ratios and composition, as reported by Fletcher et al. (2010), was never observed.

Excess ^{206}Pb from the decay of ^{230}Th is a known problem in monazite dating (Schärer 1984), particularly in Himalayan leucogranites where the melt may be rich in ^{230}Th. However, the presence of excess ^{206}Pb has not been documented in Himalayan migmatites, even in young samples where age resolution would be sufficient to detect excess of even a few %. In the present samples, no correlation was observed between apparent U–Pb age and Th/U or $^{208}Pb/^{206}Pb$. In our samples, Th–Pb ages are generally in agreement with U–Pb ages within 2 sigma. The SHRIMP was set up to measure with multipliers only, which are best suited for the lower count rates of Pb, but are unreliable for the measurement of very high count rates such as those for Th in monazite. For the above reasons, we consider U–Pb ages more accurate and we prefer them to Th–Pb ages.

Age and composition of monazite and zircon

Samples are described from south to north in the order of increasing distance from the MCT. Sample 141/01, which comes from eastern Sikkim, is an exception and it is described last. With the exception of leucosome TG9A, the crushed samples were a mixture of leucosome and mesosome. All samples contain both monazite and zircon, with the latter mineral not always recording Himalayan ages. The accessory minerals are disseminated across the matrix and are only rarely included in garnet. Therefore, the textural context is not particularly relevant for these samples. Mineral inclusions in Himalayan zircons and monazites mainly consist of quartz, apatite, and plagioclase, minerals that are present in the matrix and were equally abundant during melting or prograde metamorphism. Notably, inclusions of K-feldspar were also found in monazite from sample CLN6D, and the petrological significance of this mineral is discussed in the section on data interpretation.

The internal zoning of monazite and zircon is shown in Figs. 3 and 4. In describing the internal zoning of monazite, the core–rim terminology is used in sensu *latu*, to contrast structurally older domains (cores) that are mostly, but not exclusively, located at the center of grains, versus texturally younger domain (rims) that surround and/or truncate the cores.

Nearly all samples yield multiple date components, which are generally presented according to internal zoning (supplementary Table 1–2). The complexity of the spectrum necessarily results in a scattering of dates, despite the fact that caution was used to analyze domains wide enough to host the SHRIMP pit. U–Pb analyses and calculated dates are presented in probability diagrams and Tera-Wasserburg plots in supplementary Figs. 2 and 3. Whenever a statistically consistent group of analysis is present, an average date is reported with the relative number of analyses averaged over the total number of analyses (e.g., N 7/10). In a few samples, the dispersion of the data is well above the analytical uncertainty (MSWD > 2) and prevents calculation of an average date; in these cases, a range of dates is reported.

In this section, we also report the noteworthy features of the trace element composition of dated monazite and zircon (Figs. 5, 6; supplementary Table 3–4) with particular emphasis on the features distinguishing different domains. Ages, relevant REE signatures and Ti-in-zircon temperatures are summarized in Table 2.

In metapelite CLN5B, monazite is dominated by weak zoning organized in sectors or regular bands (cores). Occasionally, an irregular rim lacking any zoning is present; its texture suggests recrystallization of the original crystal rather than new growth (see "Discussion"). The two domains yield distinct dates and chemistry. The cores are richer in U, have a higher Th/U (2–10) and yield dates of 30–28 Ma with most analyses in a group at 28.7 ± 0.3 Ma (MSWD 1.4, N 11/14). The cross-cutting rims have systematically younger dates, mostly in the range 27–24 Ma.

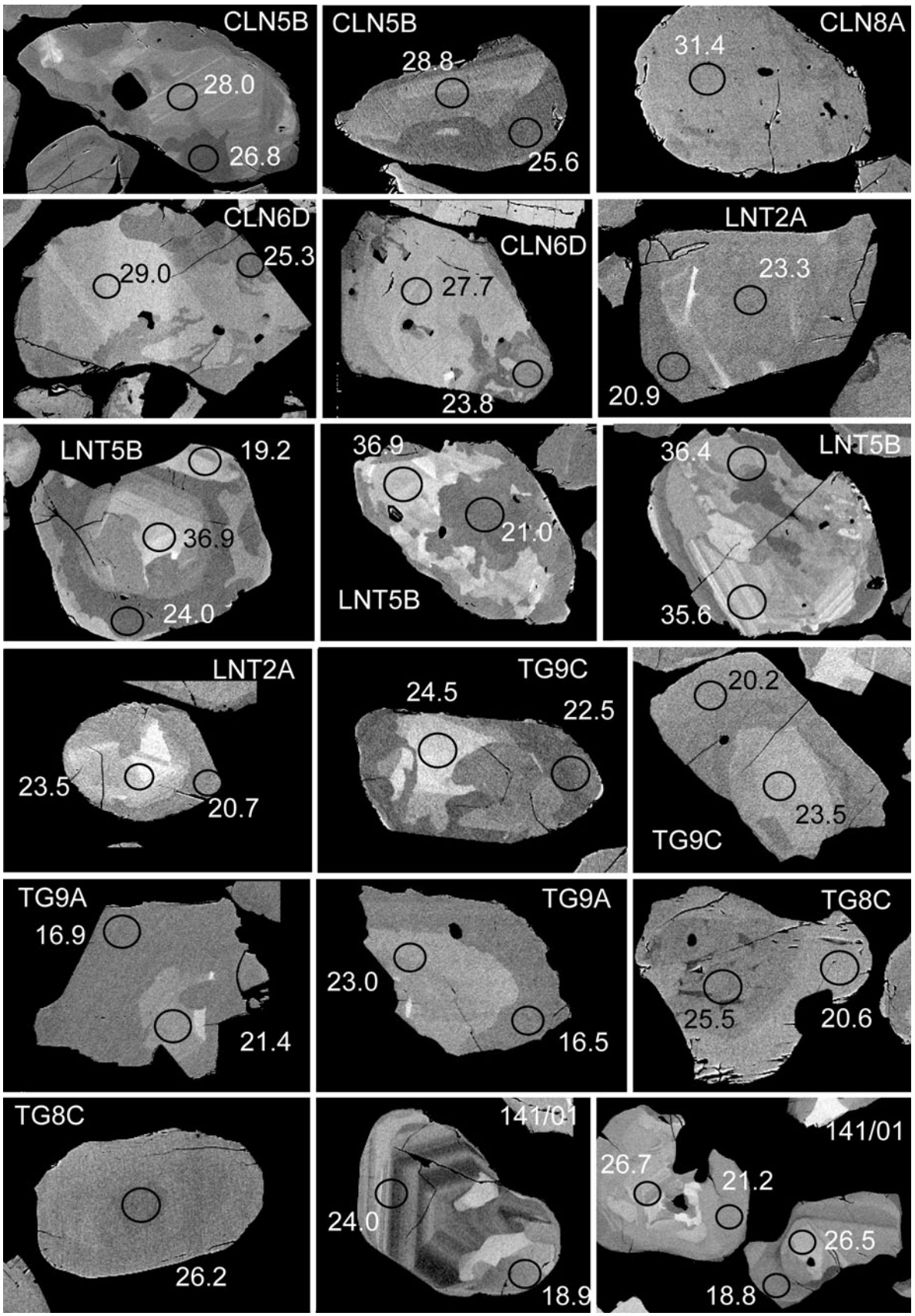
CLN5B
28.0
26.8
CLN5B
28.8
25.6
CLN8A
31.4
CLN6D
25.3
29.0
CLN6D
27.7
23.8
LNT2A
23.3
20.9
LNT5B
19.2
36.9
24.0
36.9
21.0
LNT5B
36.4
LNT5B
35.6
LNT2A
23.5
20.7
TG9C
24.5
22.5
20.2
23.5
TG9C
TG9A
16.9
21.4
TG9A
23.0
16.5
TG8C
25.5
20.6
TG8C
26.2
141/01
24.0
18.9
141/01
26.7
21.2
26.5
18.8

◀ **Fig. 3** *Back-scattered* electron images of selected monazite crystals that are representative of the crystals dated. *Circles* indicate the location of the SHRIMP analyses and are 25 μm in diameter. *Numbers* indicate $^{206}Pb/^{238}U$ ages in Ma. *Errors* on individual ages are between 1 and 2 % and thus ~0.25–0.6 Ma (supplementary Table 1)

Zircon crystals consist of cores with oscillatory zoning, which are occasionally surrounded by unzoned rims. The rims contain little Th and have low Th/U, but are not exclusively Himalayan in age (oldest rim ~860 Ma, youngest 32 Ma). The scatter of dates is likely the result of physical mixing between thin rims of different ages, and thus, an age for the Himalayan event cannot be determined.

Monazites in *metapelite CLN6D* have two domains that are distinct in zoning, chemistry and age. Unzoned to weak oscillatory domains (cores) yielded dates between 29 and 27 Ma that define a broad peak at 27.8 ± 0.3 Ma (MSWD 2.3, N 13/15). In numerous grains, the cores are cross cut by rims with patchy, irregular zoning that yield younger dates between ~25.3 and 22.5 Ma. Chemically, the cross-cutting rims are distinctly higher in HREE and Y contents and have a slightly stronger Eu anomaly (Fig. 5). Notably, a few monazite cores contain either K-feldspar or K-feldspar + quartz inclusions.

Zircons in this sample are largely constituted of detrital cores that only rarely have a thin unzoned rim, the size of which was, however, too small for SHRIMP analysis.

In metapelite CLN8A, zircons are dominated by unzoned metamorphic rims that overgrow small detrital cores. The inner rim is darker in CL and directly overgrows the cores. An external, thinner and CL-brighter rim is present in most crystals. The external rim is richer in Th, poorer in U and has a stronger Eu anomaly than the inner rim. Inner rim dates are systematically older between 31.4 and 28.6 Ma with a major peak at 30.7 ± 0.4 Ma (MSWD 1.7, N 9/12). Analyses of external rims were more difficult due to their smaller size and dates scatter between ~21.4 and 16.6 Ma with a group of 4 analyses at 20.0 ± 0.6 Ma (MSWD 1.7).

Monazite shows little internal zoning with occasional patchy domains. A few analyses on unzoned monazite confirmed the date obtained for the inner zircon rim (31.2 ± 0.4, MSWD 0.99, N 4/6).

Monazite in *metapelite LNT2A* has small cores that are irregular in shape and vary in BSE from bright to dark. The rims are unzoned and volumetrically dominant, generally euhedral and, unlike in other samples, patchy, cross-cutting domains are rare. Core and rim are distinct in date but similar in chemistry. Most core analyses yielded an average date of 23.6 ± 0.4 Ma (MSWD 0.6, N 4/5). Notably a core with a distinct zoning and a significantly higher Y and HREE content is ~30 Ma old. Monazite rims yielded dates from 21 to 19 Ma, but with a major peak at 20.7 ± 3 Ma (MSWD 1.2, N 11/17) and some additional scatter to younger dates. The monazite REE composition of rims and the 23.6 ± 0.4 Ma cores is overlapping and characterized by a strong HREE depletion (Lu_N = 10–100).

Zircons in LNT2A are dominated by euhedral weakly zoned rims that overgrow rounded detrital cores. The cores have variable CL zoning and are mostly discordant; their $^{207}Pb/^{206}Pb$ date scatter between ~2.5 and 0.5 Ga. Two distinct rims can be recognized on the basis of CL, chemistry and date. The inner rim is CL-darker, more abundant and yielded dates between 21.3 and 19.6 Ma (average 20.6 ± 0.3 Ma, N15/15, with a MSWD of 4.0 that denotes significant scatter). The external rim is brighter in CL and significantly younger at 18.4 ± 0.2 Ma (MSWD 1.7, N 13/13). Both rims have a flat HREE pattern and a strong Eu anomaly. The internal rim is, however, more strongly depleted in HREE (Lu–Gd ~1 vs. Lu/Gd 2–5 in the external rim) and has a marginally weaker Eu anomaly (Eu/Eu* of 0.08–0.11 vs. 0.07–0.08 in the external rim).

Notably, two zircon domains directly overgrowing the detrital cores returned older dates of ~24 and 32 Ma and are chemically distinct from inner and outer rims: they contain much less trace elements, are virtually Th-free and are strongly depleted in L–MREE with respect to the rims. Even though their age is not well constrained, the distinct chemistry suggests initial formation of zircon at or before ~24 Ma (cf. monazite core) in a "reactive" bulk different from the ones where the younger rims formed.

Banded metapelite LNT5B contains monazite grains that show a particularly complex internal zoning and age profile. Oscillatory domains, homogeneous crystals and homogeneous rims on variably zoned cores are all present. Patchy zoning that either cuts across the oscillatory-zoned domains or affects entire crystals is common. The dates reflect this complex zoning and show a large spread between ~39 and 16 Ma. In this distribution, the only significant peak is at 36.4 ± 0.3 Ma (MSWD 1.6) and is defined by 12 analyses, mostly on cores. The chemistry of LNT5B monazites is variable and overlaps between different age groups, but the youngest domains generally have the lowest HREE content and strongest negative Eu anomaly.

Zircons in sample LNT5B are dominated by large inherited cores with complex zoning. A small percent of crystals shows unzoned rims, but the ages of these are, however, not necessarily Himalayan (as old as ~500 Ma). Himalayan dates scatter in a similar range to that found from monazites, that is from 37 to 17 Ma, without any significant clustering.

Monazite in *metapelite TG9C* has variably zoned cores that are surrounded by euhedral, unzoned rims. Domains with mosaic zoning are only occasionally present. The distribution of dates shows a tight peak at 24.0 ± 0.3 Ma (MSWD 1.6, N 7), which included only core analyses.

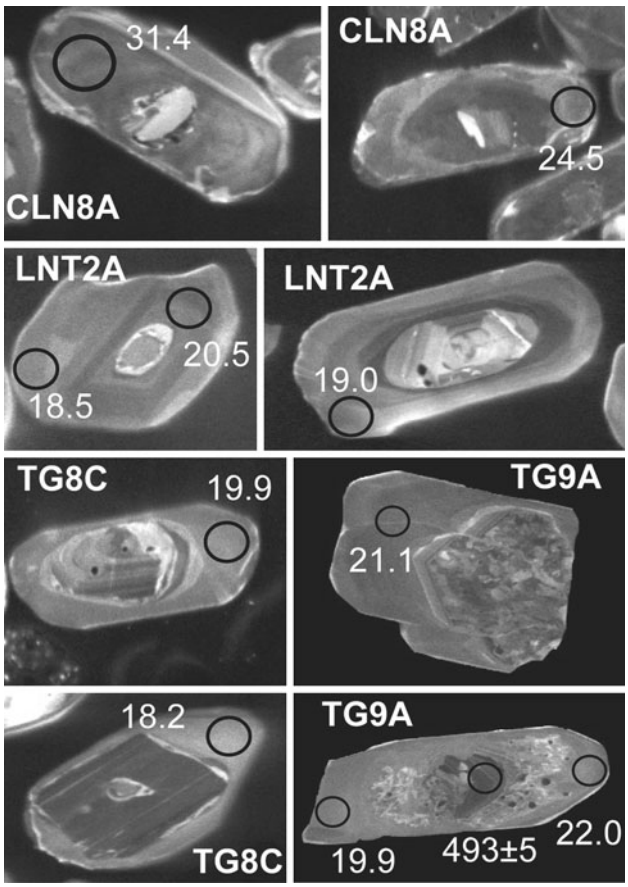

Fig. 4 Cathodoluminescence images of selected zircon crystals that are representative of the crystals dated. *Circles* indicate the location of the SHRIMP analyses and are 25 μm in diameter. *Numbers* indicate $^{206}Pb/^{238}U$ ages in Ma. *Errors* on Himalayan ages are typically ±0.3 Ma (supplementary Table 2)

Younger ages down to 22 Ma were measured in six other cores. The oldest rims analyzed define a group at 21.4 ± 0.3 Ma (MSWD 1.4, N 8/13 rims) with a tail to 17 Ma. If the youngest cores are considered within this age cluster, then the average date does not change but the scatter increases significantly (21.7 ± 0.4 Ma, MSWD 2.7, N 11). Monazite cores have a distinct chemical composition from the rims, with higher U contents (mostly 4,600–7,200 ppm vs. 1,400–2,600 ppm in rims) and a weaker negative Eu anomaly (Eu/Eu* ~0.3 vs. ~0.05 in rims). There is an increase in HREE between the monazite cores and some of the rims.

Zircons in this sample are mainly made of detrital, rounded cores, around which a thin, unzoned rim is occasionally present. Notably, the rims are themselves rounded in shape suggesting that they were resorbed. Six analyses on the largest rims yielded dates scattering between 27 and 21 Ma.

Leucosome TG9A was collected in the same outcrop as metapelite TG9C. Monazite grains are either homogeneous or display a core-rim texture. Cores preserve older ages with a cluster at 22.9 ± 0.4 Ma (MSWD 2.4, N 7/10 cores) and a tail to 21 Ma. Rims are systematically younger with most analyses forming a tight cluster at 16.7 ± 0.2 Ma (MSWD 0.66, N 7/9 rims). As for TG9C, monazite rims are richer in HREE than some cores.

Zircons have cores with a complex zoning including a peculiar mosaic zoning, as often observed in metamict or recrystallized zircons. A few analyses on cores yielded ages of ~450–520 Ma. Two distinct euhedral and weakly zoned or unzoned rims are present. The inner rim is volumetrically dominant and CL-dark and yielded an average age of 21.7 ± 0.2 Ma (MSWD 1.8, N 15/19), after matrix correction for U content (see "Methods"). The external rim is CL-bright and generally too thin for SHRIMP analyses. A single analysis on the external rim did not return an age because of the high percent of common Pb (55 %). The trace element composition of the dated rims is remarkably homogeneous with a flat HREE pattern and a notably weak Eu anomaly.

Metapelite TG8C contains monazites that are mainly homogeneous in BSE images. In a few crystals cores with patchy or faint zoning are visible. The two age peaks at 25.8 ± 0.3 Ma (MSWD 1.1, N 6) and 23.8 ± 0.3 Ma (MSWD 0.7, N 7) comprise analyses on cores and homogeneous crystals. Rims are younger and scatter in age (22–18 Ma).

The zircons in this sample have rounded detrital cores with variable zoning and are overgrown by a rounded, unzoned rim. The rim ages spread from 24.6 to 15.5 Ma. The probability diagram shows two distinct peaks at 20.2 ± 0.5 Ma (MSWD 2.2, N 7) and at 17.5 ± 0.5 Ma (MSWD 2.3, N 6). The chemistry shows no trace element difference between older and younger zircon rims, but a slight increase in Eu anomaly with decrease in age.

Sample *141/01* comes from Eastern Sikkim and contains particularly complex monazite and zircon populations. The internal zoning of monazite varies greatly and includes patchy cores or crystals, BSE-bright cores with homogeneous rims, and crystals that lack any zoning. Most of the core analyses fall within a cluster at 27.1 ± 0.3 Ma (MSWD 2.7, N 8). The age distribution shows two other tight peaks at 21.1 ± 0.2 (MSWD 0.41, N 7) and at 18.9 ± 0.2 Ma (MSWD 1.5, N7), which do not correspond to any particular zoning type.

Zircons are different from the previous samples in that they are large, euhedral crystals with oscillatory zoning. Zircon domains that are unzoned and dark in CL form embayments and rims, and surround inclusions, always crosscutting the oscillatory zoning. The oscillatory-zoned cores yielded ages spreading from 519 to 467 ± 5 Ma. They have a chemical composition typical of magmatic zircon with high Th contents and Th/U (0.1–1.0), a REE pattern enriched in HREE and with a strong Eu anomaly.

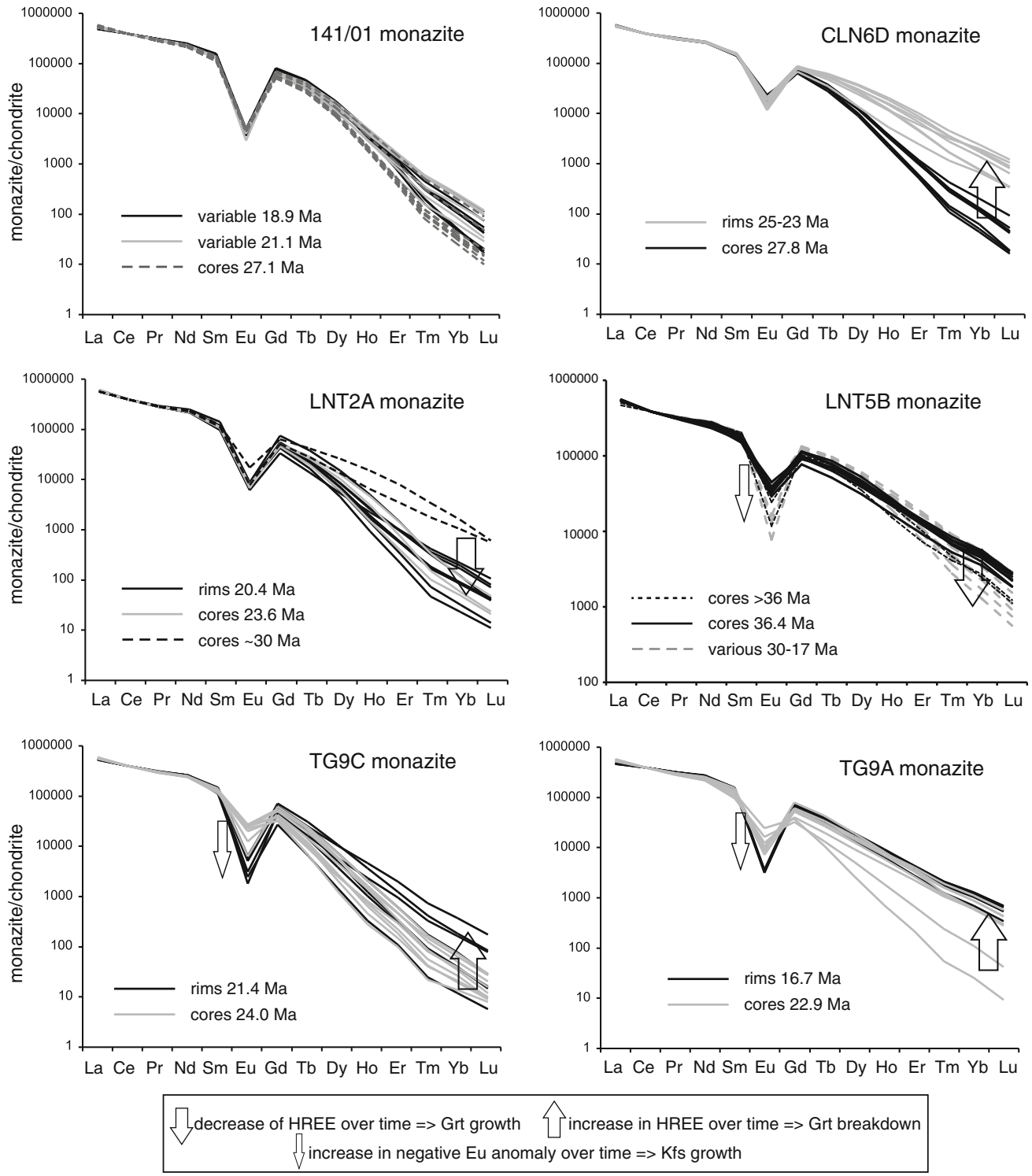

Fig. 5 Chondrite normalized diagrams of the REE composition of dated monazites. The *arrows* highlight relevant changes in REE between different growth zoned. Normalizing values from McDonough and Sun (1995)

The uniformity of the zoning, the trace element composition and the lack of any older age component suggest that the zircon cores are not detrital in origin, and the rock has a magmatic protolith of Late-Cambrian—Ordovician age. The dark domains, despite the lack of zoning, have a wide range of ages from 37 to 20 Ma. This is in line with an ample variation in HREE patterns that does not, however, correlate with age.

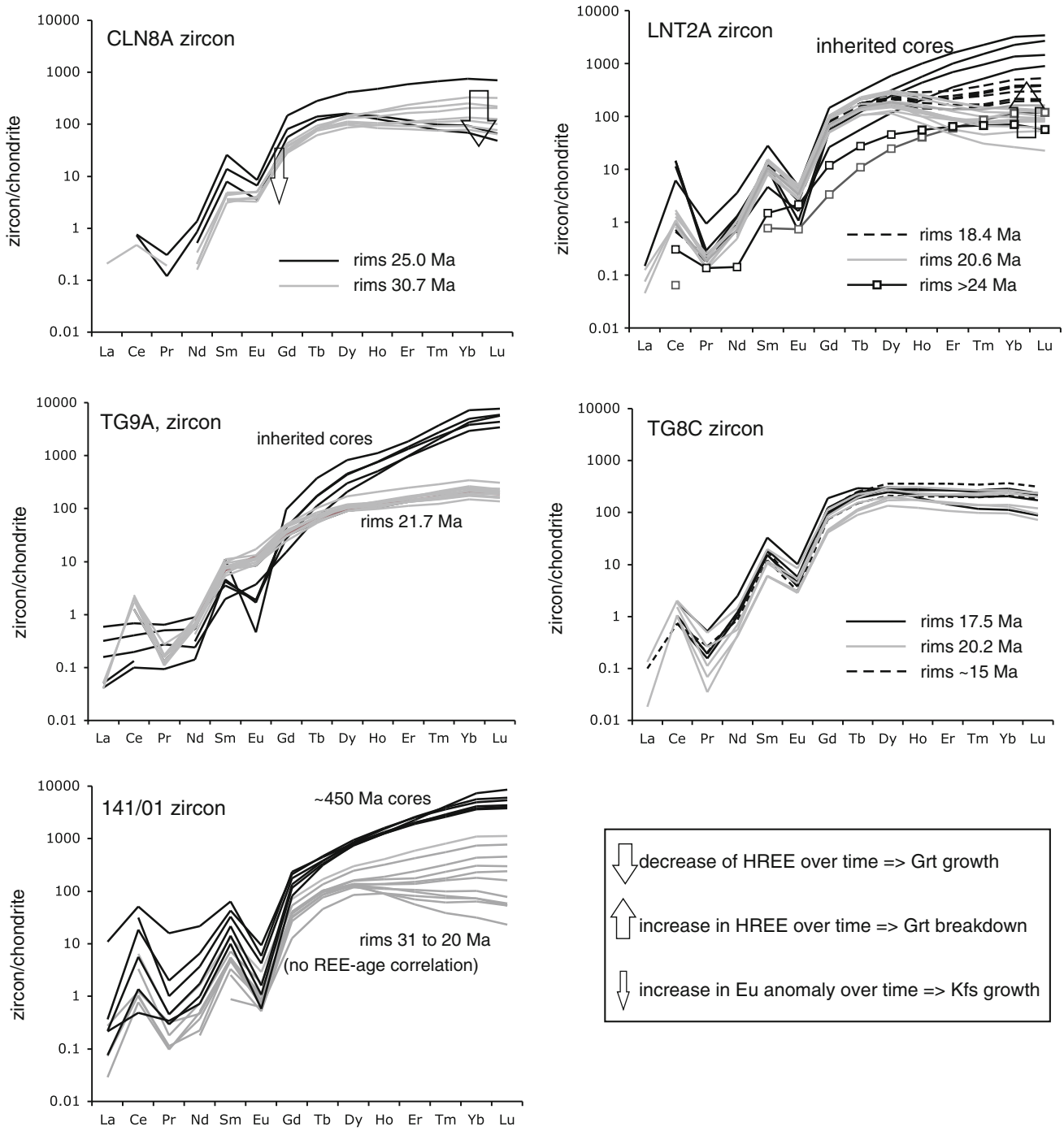

Fig. 6 Chondrite normalized diagrams of the REE composition of dated zircons. The *arrows* highlight relevant changes in REE between different growth zones. Normalizing values from McDonough and Sun (1995)

Discussion

Himalayan ages in the dated monazite and zircon spread from 36 to 17 Ma, testifying to a long-lasting metamorphism in this area (Fig. 7). If high temperatures were preserved and melting occurred over such a long period of time, new growth as well as dissolution and (re)precipitation of individual monazite and zircon grains could have occurred at any time. Additionally, any metamorphic and melting reaction may occur over a P–T range and time interval during which monazite crystallization could start, reach a peak and then tail off. In such a scenario, it is not

surprising that in some cases, monazite and zircon age populations are smeared out and that scattered dates are frequent, that is ages have a "geological scatter". Despite this, preserved domains in the monazite and zircon crystals in most samples still yield statistically consistent age clusters. This indicates that even in the most adverse conditions, the growth of accessory minerals proceeds in episodic fashion and within a short period of time that is below the resolution of our dating technique (typically ±0.3 Ma).

A rigorous interpretation of monazite and zircon ages requires that the formation of the different accessory mineral domains yielding Himalayan ages be related to specific metamorphic stages and, ideally, to specific reactions. Particularly important is to determine whether these accessory minerals formed during prograde metamorphism, melting at or around peak temperature, or during retrograde overprint at super- or sub-solidus conditions. This is chiefly relevant for monazite that, during regional metamorphism of metapelites, can readily form at sub-solidus conditions (e.g., Rubatto et al. 2001; Wing et al. 2003).

Conditions of monazite (re)crystallization

Sikkim monazites do not preserve inherited, pre-Himalayan ages. This indicates that any detrital monazite that may have been present did not survive metamorphism and all ages measured are pertinent to Himalayan metamorphism. It is still possible that monazite formed during prograde, sub-solidus metamorphism and survived anatexis. A rough estimate of the possible retention of prograde monazite in these rocks can be done considering the solubility of LREE in a granitic melt, with the assumption that monazite hosts the entire LREE of the bulk rock. The Sikkim metapelites contain ~200–250 ppm of LREE ($\Sigma_{La\text{-}Sm}$), whereas the leucosome only have ~30–70 ppm of LREE (Chakraborty, unpublished data; Neogi et al. in preparation). The latest monazite solubility data of Stepanov et al. (2012) at 10 kbar and 750–800 °C indicate that a granitic melt can dissolve ~200–350 ppm of LREE. Therefore, leucosomes (100 % melt) should not preserve any inherited monazite, and monazite preservation in the mesosome will depend on the melt/monazite ratio at the local scale. The model of Kelsey et al. (2008) also shows that if the first melt (~20 % of total melt) is lost, the LREE content of the rock will decrease and monazite dissolution will occur rapidly with increasing temperature. Therefore, solubility data suggest that in the Sikkim metapelites, prograde monazite was entirely dissolved in leucosome melts (like TG9A). Some sub-solidus monazite may have been preserved despite partial melting in mesosomes.

However, textural observations do not support the preservation of sub-solidus monazite. In the Sikkim sequence (Catlos et al. 2004) and in other amphibolite-facies metapelites (Rubatto et al. 2001; Wing et al. 2003), sub-solidus prograde monazite is generally small in size (<50 μm) and unzoned. However, monazite grains separated from the Sikkim migmatites are large (>100 μm) and show a complex internal zoning, including oscillatory bands and sectors that are most common in melt-related monazite. Additionally, the euhedral shape of most monazite grains (e.g., Fig. 3) in TG samples also suggests free growth in a melt.

The inclusion of K-feldspar in monazite from sample CLN6D dated at 28–25 Ma is further indication of formation in the presence of melt. In fact, thermodynamic considerations indicate that the modal abundance of K-feldspar would have increased significantly upon melting in the Sikkim metapelites (Fig. 8).

In summary, whereas it cannot be excluded that some sub-solidus monazite is still present in these samples, such prograde relicts should be in the form of small cores. Particularly in the samples that are rich in leucosome (LNT2A, LNT5B, TG9A, 141/01), LREE solubility, together with monazite size and internal zoning, suggests that the observed monazite formed from a melt. An exception may occur for the oldest Himalayan age (36.4 ± 0.3 Ma) that was measured in the monazite cores of sample LNT5B. This is older than the age of any melt-related zircon. On the other hand, such old monazite cores show oscillatory zoning (Fig. 3i) that is consistent with growth in a melt. This sample is in contact with an amphibolite. As documented by Faak et al. (2012), amphibolites and their immediately associated metapelites within the HHC as well as the LH differ in their appearance, assemblage and recorded P–T history from those of the far field regional metapelites. Specifically, based on petrological reasoning, Faak et al. (2012) argue for a protracted metamorphic history of these rocks that is different from that of the surrounding regional metapelites. The observation of 36 Ma monazite cores, and a diffuse age spectrum spreading to ~16 Ma, is consistent with this expectation. Given the anomalous, allochthonous stature of these rocks within the regional setting, these ages should not be interpreted in the context of regional melting events. If the 36 Ma signature dates a melting event, that would be an event that occurred at the source region of these amphibolite + metapelite package.

Retrogression is weak or absent in most samples with the exclusion of LNT samples where intense hydration occurred during retrogression. Retrograde, sub-solidus monazite formation may be possible in samples that show intense fluid alteration. According to the previous studies and experimental work (Townsend et al. 2000; Williams et al. 2011), fluid alteration of monazite leads to patchy and convolute zoning, similar to what is observed in some of the monazite grains in CLN and LNT samples (Fig. 3d, e,

Table 2 Summary of zircon and monazite ages and trace element signatures, and of zircon thermometry

Sample	Comments	Monazite age (Ma)	Monazite REE	Zircon age (Ma)	Zircon REE	Ti-in-zircon T (°C)
CLN5B	Fresh metapelite	Cores 28.7 ± 0.3, rims 27–24 Ma	na	Scatter and mixed dates 65–32	na	na
CLN6D	Fresh metapelite	Cores 27.8 ± 0.3, rims 25–22.5 Ma	Core to rim increase in HREE = garnet consumed	Not Himalayan	na	na
CLN8A	Fresh metapelite	Unzoned 31.2 ± 0.4	na	rim1 30.7 ± 0.4, rim2 25.0 ± 0.6	rim1 to rim2 decrease in HREE = garnet growth increase in Eu anomaly = K-feldspar growth	rim1 620–720 rim2 700–770
LNT2A	Metapelite with pervasive retrogression	Core ~30 Ma, cores 23.6 ± 0.4, rims 20.7 ± 3	30–23.6 Ma decrease in HREE = garnet growth	rim1 21.3–19.6, rim2 18.4 ± 0.2	rim1 to rim2 increase in HREE = garnet consumed	rim1 660–725 rim2 660–690
LNT5B	Layered metapelite associated with mafic boudin	Cores 36.4 ± 0.3, various 33–16	36–16 Ma decrease in HREE = garnet growth increase in Eu anomaly = K-feldspar growth	Scatter 37–17	na	na
TG9C	Metapelite with relict Ky	Cores 24.0 ± 0.3, rims 21.4 ± 0.3 Ma	Core to rim increase in HREE = garnet consumed increase in Eu anomaly = K-feldspar growth	Scatter 27–21	na	na
TG9A	Leucosome layer associated with TG9C	Cores 22.9 ± 0.4, rims 16.7 ± 0.2	Core to rim increase in HREE = garnet consumed increase in Eu anomaly = K-feldspar growth	rims 21.7 ± 0.2	Flat HREE = growth in the presence of garnet	660–725
TG8C	Metapelite with relic Ky	Cores 25.8 ± 0.3, rims 23.8 ± 0.3	na	rim1 20.2 ± 0.5, rim2 17.5 ± 0.5	No difference in REE	rim1 690–775 rim2 740–750
141/01	Orthogneiss from E Sikkim	Cores 27.1 ± 0.3, various 21.1 ± 0.2, various 18.9 ± 0.2	27–18 Ma increase in HREE = garnet growth	Scatter 31–20	Large variation in HREE but not correlated with age; marked negative Eu anomaly	680–780

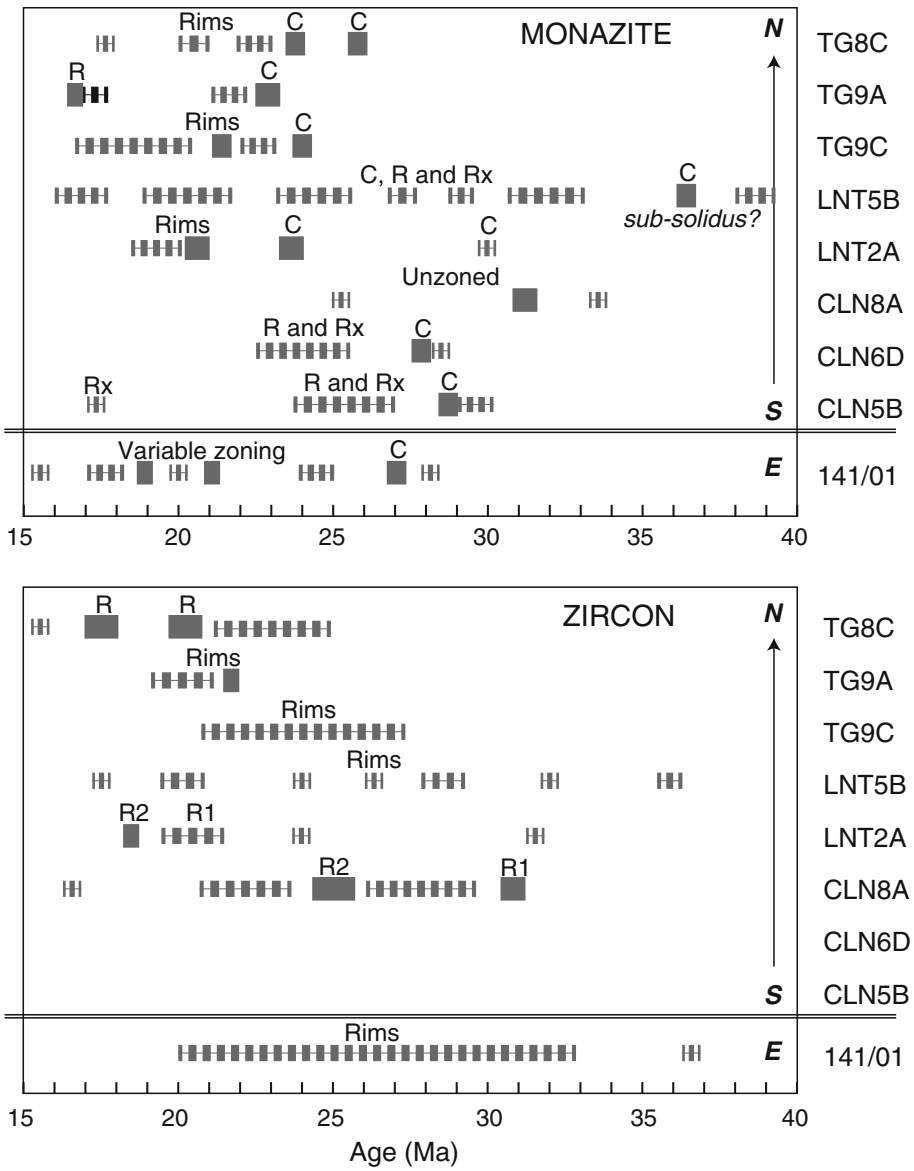

Fig. 7 Summary of $^{206}Pb/^{238}U$ monazite and zircon ages for individual samples. Ages are quoted at 95 % c.l. *C* core, *R* rim, *Rx* recrystallized domain. See text for discussion

h, i). In these samples, patchy zoned domains cross cut the regular zoning of the monazite cores that ascribed to growth during melting. The ages of the cross-cutting domains often scatter and are not amenable to average age calculation (CLN6D and LNT5B). Notably, in some cases, patchy cross-cutting domains have the same apparent age as the oscillatory-zoned cores (e.g., Fig. 3i). Such patchy zoning could have been produced by melt or fluids released upon melt crystallization as well, and these may not necessarily indicate low temperature retrogression. Overall, it is possible that in samples such as CLN5B, CLN6D and LNT5B, the late, cross-cutting domains with patchy zoning record sub-solidus recrystallization and fluid interaction rather then new growth in a melt. In Fig. 7, ages related to cross-cutting patchy domains are indicated with the prefix "Rx" and used with caution when reconstructing the timing of melting.

Zircon growth during melting

During the metamorphism of metapelites, zircon is generally not reactive before the onset of melting: that is sub-solidus zircon growth is unlikely (Rubatto et al. 2001). Whenever sub-solidus zircon formation is documented (most commonly in high-pressure samples), it has diagnostic features (e.g., Hoskin and Black 2000; Rubatto and Gebauer 2000; Corfu et al. 2003; Tomaschek et al. 2003; Rubatto et al. 2008): patchy, convolute zoning or lack of zoning, irregular shapes cross-cutting magmatic zoning and very low REE content. None of these features is present in

the dated zircon rims, which grow around rounded detrital crystals, has a euhedral shape, show weak regular zoning and has a REE pattern consistent with growth in a melt. Similar features have been reported for zircon in migmatites in numerous terranes worldwide (e.g., Vavra et al. 1999; Rubatto et al. 2001; Cottle et al. 2009b; Rubatto et al. 2009; Liu et al. 2010; Imayama et al. 2012). Alteration of zircon during retrogression is also excluded as such occurrences are rare, and again, can be recognized by texture and composition. Therefore, the zircon rims of Himalayan age are interpreted as having grown during anatexis between ~31 and 17 Ma, the same period during which the growth of most monazite occurred.

Support for zircon growth during melting comes from Ti-in-zircon thermometry (Watson et al. 2006). Assuming a TiO_2 activity of 0.5 (ilmenite present), the temperatures range from 670 to 760 °C (Table 2 and supplementary Fig. 4). The calculation is affected by some uncertainty about the activity of TiO_2, which cannot be exactly determined in a dynamic melting environment. Despite such uncertainty, the obtained temperatures are in the range expected for melting. According to the calculation and modeling of Socar et al. (in preparation), the Sikkim metapelites underwent fluid-induced and muscovite dehydration melting at ~700–750 °C (P of 7–8 kbar), followed by biotite melting initiated at ~750 °C. The spread of Ti content within a single zircon population, the uncertainty in TiO_2 activity and the errors associated with the Ti-in-zircon thermometer prevent determining whether outer and inner zircon rims within the same sample (CLN8A, LNT2A, TG8C) formed at different temperatures.

Chemical indicators for different melting reactions

The comprehensive data set presented here allows assessing whether, during the extended period of melting (~31–17 Ma), it is possible to time the different reactions or stages of melting. Whereas zircon composition may fail to vary significantly when in equilibrium with melts produced by different reactions, in an anatectic environment, zircon and monazite may reflect the appearance and disappearance of other trace element-bearing phases like garnet for Y and HREE, and feldspars for Eu (Schaltegger et al. 1999; Foster et al. 2002; Rubatto 2002).

Garnet is ubiquitous in the investigated samples (Figs. 2, 7a): it forms during prograde sub-solidus metamorphism and survives as restitic phase during melting and can even be a peritectic phase. The amount of garnet present drops sharply during decompression (i.e., garnet breaks down, forming corona assemblages involving phases such as cordierite, spinel, plagioclase, with/without production of new melt) and initial cooling at lower pressures. This behavior is expected from petrogenetic grids (Spear et al. 1999) and observed in thin section (Fig. 2a–d).

Because garnet is the main host for HREE in these metapelites, variations in the HREE content of monazite or zircon within a sample (Figs. 5, 6; supplementary Table 3–4) will depend on the amount of garnet present in the rock. The variation in the volume of garnet in two representative samples is modeled in Fig. 8b, c: garnet increases in volume during the prograde path and decreases drastically during isothermal decompression and then cooling. Monazites in two samples (LNT2A and LNT5B) show a sharp to moderate decrease in HREE from core to rim (Fig. 5; Table 2). Zircon in sample CLN8 also shows decrease in HREE from the inner to the outer rims. These chemical variations, thus, time the increased garnet growth during prograde to peak metamorphism, namely from 28–30 to 25 Ma in CLN samples and 30–23.6 Ma in LNT2A.

Garnet consumption during decompression liberates HREE and in turn leads to increased HREE content in accessory minerals. A marked increased in HREE is present in sample CLN6D from the ~27.8 monazite cores to 25–23 Ma rims, and in LNT2A, from the inner ~20.6 Ma rims to the outer ~18.4 Ma zircon rims. Similar variations are present in TG9A and TG9C monazites between 24 and 23 Ma cores and 21–17 Ma rims. Breakdown of garnet during decompression and initial cooling is also documented by the HREE composition of zircon in migmatites of the HHC in eastern Nepal (Tamor-Ghunsa section), ~50 km west of Sikkim (Imayama et al. 2012).

Because of garnet resorption and retrogression in the investigated samples, garnet rims that formed at peak conditions are not present anymore. Limited diffusion of REE in zircon (Cherniak 2010) as well as garnet would prevent zircon from equilibrating with newly exposed garnet rims. This complexity prevents the use of zircon/garnet equilibrium partitioning to correlate monazite and zircon REE compositions with a specific garnet zone (Hermann and Rubatto 2003).

Negative Eu anomaly (Eu/Eu*) can be similarly used as indicator of feldspar production. In these rock types, only feldspars are capable of fractionating Eu from the REE. Among the feldspars, K-feldspar has a stronger positive Eu anomaly than plagioclase (Bea et al. 1994) and produces a stronger negative Eu anomaly in coexisting phases (see garnet in Buick et al. 2010). In this bulk rock composition, K-feldspar is not present until melting begins and the modal volume of K-feldspar increases rapidly at ~760–780 °C upon biotite melting (Fig. 8d, e). The presence of K-feldspar inclusions in monazite domains dated 28–25 Ma in sample CLN6D is thus direct indication of the presence of melt at that time. In all metapelitic

samples, there is a general trend to a stronger negative Eu anomaly (decrease in Eu_N/Eu_N^* values in Fig. 9) at younger ages. This correlation is particularly strong in CLN8A and TG8C zircons, and TG9A and TG9C monazite. Whereas there can be a bulk compositional control on the amount of feldspar produced, the Eu anomaly–age trend suggests that, after initial melting, biotite melting and K-feldspar production was dominant at around 23–21 Ma.

Therefore, based on the evolution of the abundances of major phases that affect the REE content of monazite and zircon, the P–T history of Sikkim pelitic migmatites can be divided into three segments (Fig. 8):

1. T increasing—garnet increases, K-feldspar increases
2. T constant, P drops—garnet decreases, K-feldspar is roughly constant
3. T decreases at low P—garnet decreases slightly, K-feldspar decreases.

The last stage may not be recorded in accessory phases such as monazite or zircon because temperatures may be too low for the growth of these phases. The different groups of metapelitic migmatites (CLN 5B, 6D, 8A; TG 9C, 9A, 8C and LNT 2A) studied in this work record these stages, as discussed below.

Regional age trend and distinct migmatite types

In the age summary of Fig. 7, there is a jump in zircon and monazite ages from CLN (ages of populations between ~32 and 22 Ma) to TG samples (ages between 26 and 17 Ma). Main phase petrology together with age and chemical signature of zircons and monazites (Table 2) are combined to reconstruct the P–T–time evolution of the two units (Fig. 8a), which is summarized below.

CLN sequence

~31–28 Ma, monazite starts to form during prograde metamorphism, possibly as early as paragonite melting (~580 °C) and proceeding into muscovite dehydration melting. Low volume of K-feldspar and garnet would have been present at this stage as monazite has small negative Eu anomaly (CLN8A) and relatively high HREE content (LNT2A). Monazite in CLN8A, first zircon rim in CLN8A, and monazite cores in CLN5B and LNT2A record this stage. From 28 to 25 Ma, zircon and monazite grow during abundant melting close to the peak of metamorphism. K-feldspar increases significantly by biotite melting (K-feldspar inclusion and increase in negative Eu anomaly in CLN6D monazite) and garnet is a dominant phase (low HREE content in CLN6D monazite cores and the outer zircon rim in CLN8A). Toward the end of decompression and during cooling (~25 Ma and after), significant garnet dissolution leads to an increase of HREE in the system. This stage is mainly recorded in CLN6D monazite rims.

TG sequence

The same chemical signatures as observed in the CLN samples are present in the TG samples but at later times. At 26–23 Ma, monazite and zircon crystallize during the prograde path, in a garnet-rich assemblage (low HREE contents in monazite cores of TG9 samples and in zircon rims). Melting is limited as signatures due to the presence of K-feldspar are virtually absent. Between 23 and 20 Ma, there is significant zircon growth during increasing melt production (increasing Eu anomaly) at peak. Zircon and monazite rims in TG9 and TG8 grew during this stage. After 20 Ma, toward the end of decompression, decrease in T produced retrogression of garnet and a second rim in accessory minerals (higher HREE in TG monazite rims and LNT2A zircon) until ~17 Ma.

Despite the similarities in P–T evolution, the P–T–time paths of the two sequences reveal some important features: 1) the southern CLN unit reached peak metamorphism significantly earlier than the TG unit; 2), the duration of decompression in any given rock in the two units is similar (~3 Ma); 3) the two units came together at the end of decompression during cooling, after they reached mid to upper crustal conditions (~5 kbar). Diachronicity of melting and different heating/exhumation rates between different portions of the HHC have important implications for understanding the tectonics of this region (see "Discussion" below). A similar diachronous metamorphism across the HHC has been recently reported in nearby eastern Nepal (Imayama et al. 2012). In that area however, the sample at a higher structural level and metamorphic grade recorded earlier metamorphism (33–23 Ma) than the southern, lower grade sample (21–16 Ma). This trend is opposite to the one we document in the Sikkim area between the CLN (structurally lower, older) and the TG sections (structurally higher, younger). A similar age trend, with younger metamorphic rocks thrusted over older rocks, has been reported in NW Buthan (Warren et al. 2011), but that evolution is younger than in Sikkim (13–15 Ma in the north and 17–21 in the south).

We suggest that the younging trend in Sikkim is due to decoupling between the northern and southern part of the HHC in Sikkim during their evolution. This implies a tectonic discontinuity north of Lachen (~27°45′ N, Fig. 1). Field and petrographic observations support this scenario. The section between Lachen and Thangu is strongly deformed and characterized by hydrous retrogression (e.g., sillimanite not preserved, retrograde chlorite replacing garnet, sericite and fine-grained white mica

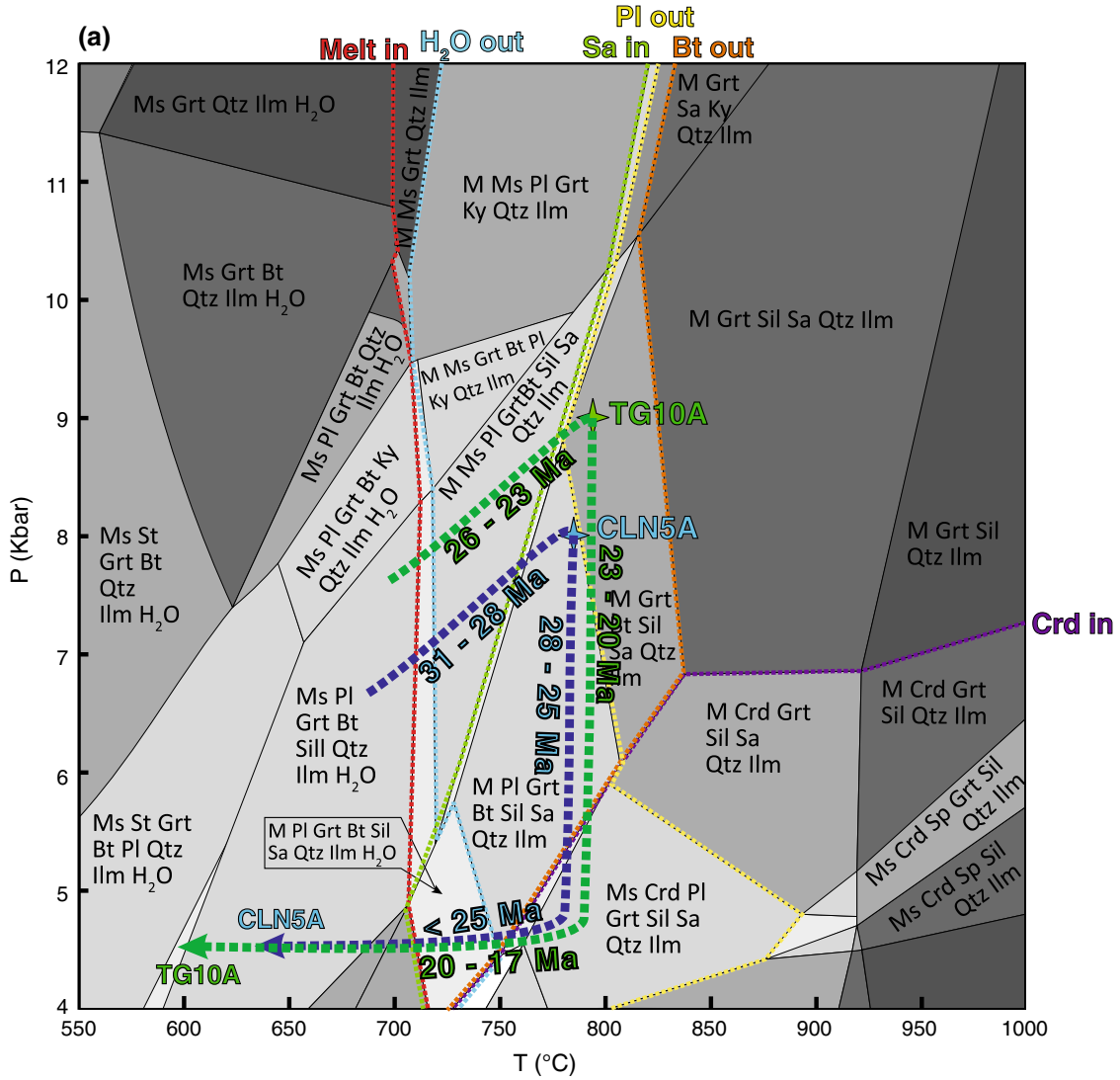
(a)
Melt in
H2O out
Pl out
Sa in
Bt out
Ms Grt Qtz Ilm H2O
M Ms Grt Qtz Ilm
M Grt Sa Ky Qtz Ilm
M Ms Pl Grt Ky Qtz Ilm
Ms Grt Bt Qtz Ilm H2O
M Grt Sil Sa Qtz Ilm
Ms Pl Grt Bt Qtz Ilm H2O
M Ms Grt Bt Pl Ky Qtz Ilm
M Ms Pl GrtBt Sil Sa Qtz Ilm
TG10A
Ms Pl Grt Bt Ky Qtz Ilm H2O
26 - 23 Ma
CLN5A
23 - 20 Ma
Ms St Grt Bt Qtz Ilm H2O
M Grt Sil Qtz Ilm
Crd in
31 - 28 Ma
28 - 25 Ma
M Grt
t Sil
a Qtz
m
Ms Pl Grt Bt Sill Qtz Ilm H2O
M Crd Grt Sil Sa Qtz Ilm
M Crd Grt Sil Qtz Ilm
M Pl Grt Bt Sil Sa Qtz Ilm
Ms St Grt Bt Pl Qtz Ilm H2O
M Pl Grt Bt Sil Sa Qtz Ilm H2O
Ms Crd Sp Grt Sil Qtz Ilm
Ms Crd Sp Sil Qtz Ilm
CLN5A
< 25 Ma
Ms Crd Pl Grt Sil Sa Qtz Ilm
TG10A
20 - 17 Ma
P (Kbar)
T (°C)

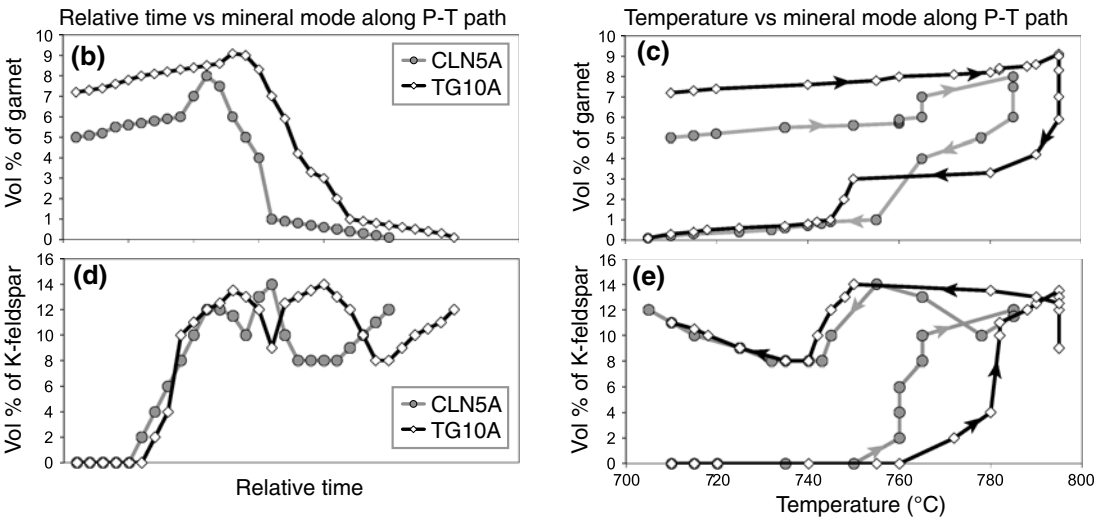
Relative time vs mineral mode along P-T path
(b)
CLN5A
TG10A
Vol % of garnet
(d)
Vol % of K-feldspar
Relative time
Temperature vs mineral mode along P-T path
(c)
(e)
Temperature (°C)

◀ **Fig. 8** P–T-time path for the Sikkim migmatites. **a** Pseudosection and thermobarometric results calculated by Sorcar et al. (in preparation) for rocks from the same region and outcrops. The pseudosections were calculated in the system MnNCKFMASH using Holland and Powell (2001) database and the Perplex software for a typical migmatite bulk composition from North Sikkim. The peak (~800 °C) and retrograde (~600 °C) metamorphic P–T conditions obtained by kinetically constrained individual thermobarometry are superposed on the topology of the phase diagram. The CLN and TG samples follow similar P–T paths, with the CLN samples attaining slightly lower pressures of metamorphism. The prograde P–T path is poorly constrained and is drawn to indicate an increasing P–T trend that may be expected in a collisional setting. The isothermal decompression and isobaric cooling segments of the paths are well constrained by reaction textures and thermobarometry. Association of isotopic dates to different segments of the P–T paths is based on the discussion in the text. *M* melt, other mineral abbreviations according to Kretz (1983). Contouring the stability fields with modal abundances allows the evolution of abundance of individual minerals (or melt) along a P–T path to be constructed. **b** The evolution of abundance of garnet in two rock samples as a function of relative time as a rock traverses the P–T path, in **c** the same data are illustrated as a function of temperature evolution along the P–T path. **d**,**e** the evolution of K-feldspar abundance at the same stages of evolution of the rocks. See **b** and **c** for legend

replacing K-feldspar, and green biotite + ilmenite replacing HT biotite). Patchy zoning indicative of fluid alteration (Townsend et al. 2000; Williams et al. 2011) is particularly abundant in monazites from the LNT samples. Most notably, the CLN and TG samples have different cooling histories (Sorcar et al. in preparation). These observations now help to place metapelite LNT2A that occurs between these two blocks, in context. The hybrid nature (LNT2A has old monazite cores as in CLN, but most of accessory mineral growth occurs simultaneously with TG samples) and higher retrogression and deformation indicates that LNT marks a region of discontinuity and ductile faulting between CLN and TG.

In addition to the regional trend, individual samples from the same unit or even outcrop may record zircon and monazite crystallization from melt at slightly different times (compare TG8 with TG9). These age differences could arise from differences in "reactive" bulk inducing LREE and Zr saturation at different times (Kelsey et al. 2008) and/or sample following a slightly different P–T evolution and thus melting history. As for the other Tertiary collisional belts (Rubatto et al. 2009), the young age and good precision allow resolving these slight age differences in the Himalayan migmatites, which can be missed in older terranes. These data highlight the risk of attributing the age of anatexis by dating only one or a few samples.

Sample 141/01 in SE Sikkim records zircon and monazite formation over an extended period of time that overlaps with both portions along the N–S transect. This chronology confirms that metamorphism in eastern Sikkim was roughly synchronous with rest of the HHC in the region. The limited data for this area, as well as different nature of the protolith (an orthogneiss rather than a pelitic migmatite), do not allow evaluating whether the same

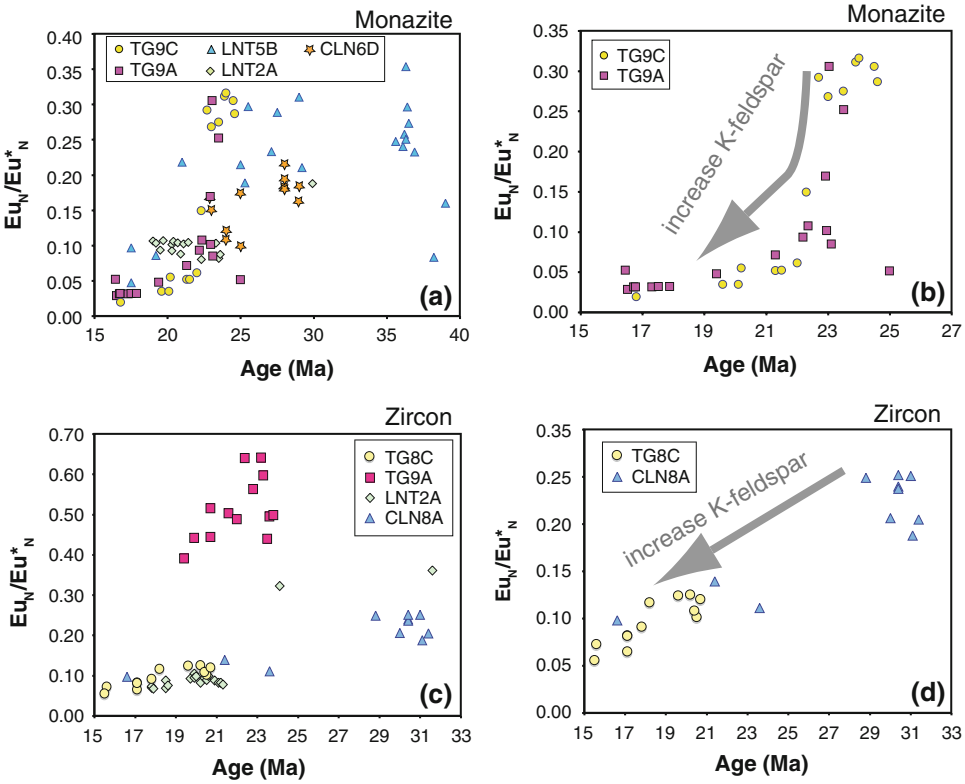

Fig. 9 Binary plots of individual monazite (**a**, **b**) and zircon (**c**, **d**) ages versus Eu anomaly [Eu/((Sm + Gd)/2), all values normalized to chondrite] as proxy for K-feldspar growth. Plots **a** and **c** show all samples, whereas plot **b** and **d** show selected samples where the correlation is particularly strong. Only metapelitic samples and related leucosomes are plotted. See text for discussion

discontinuity that is present in the N–S section also occurs in the eastern flank of the Sikkim structure. However, the protracted monazite and zircon record in orthogneiss 141/01 with respect to individual metapelitic samples in the north raises the possibility of different protolith behaviors or different thermal evolutions between the HHC in the north and on the flank of the Sikkim structure.

Geochronology of Himalayan HT metamorphism—a hierarchy of timescales

Age constraints on metamorphism within the HHC are particularly abundant for the central part of the Himalayan chain (Tibet and Nepal) and around the Everest region (see a review in Jessup et al. 2008), whereas only a couple of works refer to the region of Sikkim (Catlos et al. 2004; Harris et al. 2004). The majority of Himalayan geochronology has, however, targeted the various tectonic discontinuities with the aim of timing the tectonic movements. Systematic investigation of continuous metamorphic sequences or large uniform provinces is limited to a few studies (Cottle et al. 2009b; Warren et al. 2011; Imayama et al. 2012).

Despite uncertainties in the interpretation of some ages, a general picture emerges for the overall evolution of the Himalayan chain. The early stages of metamorphism have been dated at between ~44 and 36 Ma in various parts of the chain: greenschist facies metamorphism and garnet growth at 44–36 Ma in Nanga Parbat (Foster et al. 2000); early garnet growth at ~43 Ma, and kyanite–garnet metamorphism at ~39 Ma in the Dolpo region, Western Nepal (Carosi et al. 2010), prograde metamorphism in the Everest region at ~39 Ma (Cottle et al. 2009a). An age of peak metamorphism of ~32 Ma has been proposed for the Everest region (Simpson et al. 2000). Evidence of melting in these early stage of metamorphism are rare: melting at relatively high pressures in the kyanite field is documented in the MCT Zone of E Nepal and dated at ~31 Ma (Groppo et al. 2010) and possibly at ~35 ± 3 Ma in central Nepal (Godin et al. 2001). Temperatures consistent with melting have recently been reported in central Nepal, Annapurna region, where high temperature titanite ranges in age from 37 to 20 Ma (Kohn and Corrie 2012). A number of workers refer to this first stage as "Eohimalayan" M1 metamorphism (Vance and Harris 1999; Simpson et al. 2000; Godin et al. 2001), to distinguish it from a later phase at lower pressure in the sillimanite stability field.

Abundant geological constraints across the central and eastern part of the Himalaya (Simpson et al. 2000; Viskupic et al. 2005; Jessup et al. 2008; Kellett et al. 2010) indicate that sillimanite-garnet grade metamorphism occurred broadly in the period 26–20 Ma, and possibly as early as 28 Ma (Cottle et al. 2009b). At the higher structural levels (MCT Zone and HHC), pervasive partial melting occurred from ~23 Ma (Viskupic et al. 2005; Warren et al. 2011) until the Middle Miocene together with widespread granite emplacement across the Himalayan chain. A single study just west of Sikkim reported migmatisation from early Oligocene and that extended over a period of time that is similar to the interval that we document (33–16 Ma, Imayama et al. 2012).

Little of this evolution has been documented in the Sikkim region where geochronology was limited. Dating of garnet in a leucosome in west Sikkim returned imprecise ages at 23.0 ± 2.6 Ma for the core and 16.1 ± 2.4 for the rim, which were interpreted as dating prograde-peak metamorphism and decompressional melting (Harris et al. 2004). A geochronologic study of monazites (Catlos et al. 2004) had a structural scope (time of movement along the MCT Zone) and, in that study no information was sought in the internal structure and composition of monazites. Such an approach likely resulted in the mixing of different age components and could not possibly resolve any P–T stages represented by multiple monazite domains.

Our data set indicates that melting in the HHC was already occurring by 31 Ma (the age of the oldest zircon overgrowth) and lasted until ~17 Ma, the age of the youngest zircon and monazite rims. This longer time span covers both the time of peak metamorphism and HP melting in the kyanite field (Godin et al. 2001; Groppo et al. 2010) and that of HT melting and granite emplacement (Viskupic et al. 2005; Cottle et al. 2009a). There is no time gap between these events that were previously considered distinct, leading to the conclusion that the Eo-Himalayan and Meso-Himalayan distinction cannot be applied to Sikkim. The same applies to the HHC in eastern Nepal (Imayama et al. 2012), and it may be necessary to reconsider the distinction for other regions where earlier signs of high temperature melting are documented (Cottle et al. 2009b).

The combination of textural, geochemical and petrological criteria with isotopic dates in this study reveals a picture of subtle complexity involving diachroneity and a hierarchy of timescales of melting in the HHC in this region: Melting over the entire HHC occurred over a period of about 15 million years (31–17 Ma). However, this melting occurred in different blocks at different times (e.g., CLN vs. TG) with discontinuities between these blocks (e.g., LNT). A given block traversed the P–T region of melting within 5–7 million years. Within a block, specific melting reactions may have been intersected at slightly different times by different pieces (e.g., different samples of CLN or TG), leading to a real, geological scatter in the age spectrum of a given accessory mineral (with a given trace element signature and texture), in addition to

analytical uncertainties. Furthermore, it could be shown that allochthonous blocks or different protoliths, recording a different evolutionary history, could be embedded within the regional stratigraphy (sample LNT5B), and therefore, the dating of single, isolated samples could be misleading.

The implications of these results for the calculation of cooling and exhumation rates may now be considered. The timescales of 5–7 Ma for traversing the P–T field or melting (>700 °C, up to ~10 kbar, decompression to mid-crustal depths for about 5 kbar followed by cooling below ~700 °C) match the duration obtained from geodynamic modeling (Faccenda et al. 2008). Such a timescale is also consistent with geospeedometric constraints (Sorcar et al. in preparation). These results are not consistent with a duration of ca. 7 Ma (23–16 Ma) for decompression alone that has been inferred based on somewhat uncertain dates of garnets (Harris et al. 2004), or slow cooling rates of 15–40 °C/Ma that have been inferred by combining zircon dates with FT ages (Imayama et al. 2012).

Implications for Himalaya tectonics

The presence of early, >25 Ma old melting during prograde metamorphism, as well as diachronicity between different portions of the HHC, has important implications for tectonic models. First of all, the association of dates to different segments of the P–T paths (Fig. 8a) shows that melting occurred before decompression and, therefore, drop in density and exhumation may be the consequence of melting rather than the other way around (e.g., Harris et al. 2004). This inference is similar to that of Viskupic et al. (2005) and Groppo et al. (2010).

Channel flow has been proposed as a major process to explain the tectonics, P–T paths and timing of the Himalayan orogen (e.g., Beaumont et al. 2004; Jamieson et al. 2004; Godin et al. 2006). Application of a typical thermo-mechanical numerical model to the HHC successfully reproduced the shape of the P–T paths observed across the region (Jamieson et al. 2004), including the isothermal decompression that characterized the Sikkim HHC granulites (Ganguly et al. 2000; Sorcar et al. in preparation). One of the main features of a channel flow model is the synchronous evolution of different parts of the sequence, with lower and higher structural levels reaching peak T and P at the same time (see Fig. 4 in Jamieson et al. 2004). Unlike absolute timing, synchronicity is a necessary condition of the models in their present form, and this feature does not depend on the initial radiogenic heat flow, plate velocity or properties of the crustal layers chosen for the model. The P–T–time data presented here, in particular the diachronicity between CLN and TG units, cannot be reconciled with simple channel flow models. It is noteworthy that, without the time information, the two segments of the HHC identified here would show very similar P–T path and be in line with synchronous evolution across the HHC. As shown elsewhere, single ages of HHC samples would not be sufficient to resolve diachronicity and would still be compatible with channel flow (see an example in Kellett et al. 2010).

Simultaneous movement along the MCT and the STDS during the Miocene (~24–16 Ma) has been widely proposed as playing a major role in the exhumation of the HHC (Godin et al. 2006). The P–T–time history of the Sikkim migmatites (Fig. 8) indicates that (i) in the region between the MCT and the STDS, different rock units underwent exhumation at different time and rates, with a further discontinuity between them and that (ii) in the unit closer to the MCT, significant exhumation was already occurring from ~27 Ma. Future studies will have to explore the possibility that the two main tectonic discontinuities acted separately and carried distinct rock packages. The identification of this additional discontinuity within the HHC alters the equations for balancing the extent of convergence, compression and exhumation.

A structural discontinuity within the HHC has been reported in central Nepal (Martin et al. 2010) as well as in western Nepal (Toijen shear zone, Carosi et al. 2010), and its initial activity has been dated at ~26 Ma, before the onset of movement so far detected along the MCT. A break in grade and age of metamorphism marked by a tectonic discontinuity has also been identified in NW Bhutan (Warren et al. 2011; Grujic et al. 2011), but interestingly, in that section, the age of decompression from granulite facies along the thrust is as young as 15–13 Ma. The LNT section of the Sikkim migmatites could represent a similar shear zone and determining the timing of movement on it, and its nature is crucial for future tectonic models of the HHC.

Conclusions

Determination of age using zircon and monazite in nine samples of migmatites indicates that within one metamorphic cycle, these minerals may record different stages/reactions. This results in a complex distribution of dates that can only be correctly resolved and interpreted by dating of multiple domains, paying attention to their relative sequence, and combination of geochronology with P–T paths, reaction sequences and related trace element changes in accessory minerals.

With this multidisciplinary approach, U–Pb ages from the Sikkim migmatites can be related to metamorphic stages within a complex tectonic setting. Monazite and zircon growth zones record a protracted melting and HT history in the HHC of Sikkim from ~31 to 17 Ma. An older ~36 Ma high-grade event is recorded in an allochthonous relict related to mafic lenses.

The variation of trace element composition of the dated growth zones is indicative of changes in the coexisting assemblages and, in turn, melting reactions. Changes in HREE and negative Eu anomaly record garnet growth during prograde metamorphism, biotite dehydration melting with the production of K-feldspar and garnet resorption during decompression and cooling. These metamorphic stages did not occur at the same point of time in different segments of the HHC in Sikkim along a N–S transect.

Such combined analysis of texture (i.e., core vs. rim, or cross-cutting relations, yielding relative sequence of events), trace element geochemistry and isotopic dates reveals a hierarchy of timescales during the crustal melting in a region: while melting lasted about 15 Ma across the HHC (an event), any given block traversed the melting field in 5–7 Ma, and within the blocks, individual rock samples may have experienced the same reactions that lasted much shorter, at slightly different times (episodes).

The age distribution across the N–S transect, combined with field and petrographic observations, suggests a decoupling between the northern portion at higher structural levels and the southern portion of the HHC. The two units record a similar, but not simultaneous, metamorphic path: high-grade metamorphism and melting started earlier, from 31 Ma, in the southern portion (Chungthang to Lachen, CLN), which then underwent earlier decompression with respect to the northern portion (north of Thangu, TG). The two units became coupled only at the onset of cooling after 20 Ma.

Diachronous metamorphism and different cooling rates of units within the HHC cannot be reconciled with a channel flow model in its most basic form, which requires synchronous evolution across the HHC. The region is an amalgamation of at least two units that were mobile at different points in time and were eventually juxtaposed. Absolute and relative timing of metamorphism also demand the presence of a regional tectonic discontinuity within the core of the HHC that was active before the currently recorded periods of movements along the MCT. This requires that models of compression, convergence and exhumation consider the role of such discontinuities in reconstructing the tectonic evolution of the orogen. The heterogeneity of spatial and temporal distribution of melting makes it a challenge to estimate the amount of melt present at a given point of time and its influence on exhumation and tectonics.

Acknowledgments Field work in Sikkim and data interpretation benefited from constructive and animated discussions with Robert Anczkiewicz and Dilip Mukhopadhyay. Michaela Flanigan and Mike Jolland (ANU) are thanked for compiling chemical data and petrographic observations, respectively. The review of C Warren and B Bingen is kindly acknowledged. D Rubatto was financially supported by the Australian Research Council, QEII fellowships, DP0556700 and DP110101599. The research of S Chakraborty is supported by funds from the DFG and the Ruhr Universitaet Bochum. S Dasgupta acknowledges the financial support of the DST, Government of India, through the J.C. Bose Fellowship.

References

Acharryya SK, Ray KK (1977) Geology of the Darjeeling-Sikkim Himalaya, guide to excursion no. 4, International Gondwana Symposium. Geological Survey of India, p 25

Aleinikoff JN, Schenck WS, Plank MO, Srogi L, Fanning CM, Kamo SL, Howell B (2006) Deciphering igneous and metamorphic events in high-grade rocks of the Wilmington Complex, Delaware: morphology, cathodoluminescence and backscattered electron zoning, and SHRIMP U-Pb geochronology of zircon and monazite. Geol Soc Am Bull 118(1/2):39–64

Bea F, Pereira MD, Stroh A (1994) Mineral/leucosome trace-element partitioning in a peraluminous migmatite (a laser ablation-ICP-MS study). Chem Geol 117:291–312

Beaumont C, Jamieson RA, Nguyen MH, Medvedev S (2004) Crustal channel flows: 1. Numerical models with applications to the tectonics of the Himalayan-Tibetan orogen. J Geophys Res 109:B06406. doi:10.1029/2003JB002809

Black LP, Kamo SL, Allen CM, Aleinikoff JM, Davis DW, Korsch RJ, Foudoulis C (2003) TEMORA 1: a new zircon standard for Phanerozoic U-Pb geochronology. Chem Geol 200:155–170

Buick IS, Clark C, Rubatto D, Hermann J, Pandit M, Hand M (2010) Constraints on the proterozoic evolution of the Aravalli-Delhi Orogenic belt (NW India) from monazite geochronology and mineral trace element geochemistry. Lithos (in press)

Butera KM, Williams IS, Blevin PL, Simpson CJ (2004) Zircon U-Pb dating of early palaeozoic monzonitic intrusives from the Goonumbla area, New South Wales. Aust J Earth Sci 48:457–464

Carosi R, Montomoli C, Rubatto D, Visona' D (2010) Late oligocene high-temperature shear zones in the core of the Higher Himalayan crystallines (Lower Dolpo, western Nepal). Tectonics 29:TC4029. doi:10.1029/2008TC002400

Catlos EJ, Harrison TM, Manning CE, Grove M, Rai SM, Hubbard MS, Upreti BN (2002) Records of the evolution of the Himalayan orogen from in situ Th-Pb ion microprobe dating of monazite: Eastern Nepal and western Garhwal. J Asian Earth Sci 20(5):459–479

Catlos EJ, Dubey CS, Harrison TM, Edwards MA (2004) Late Miocene movement within the Himalayan Main Central Thrust shear zone, Sikkim, north-east India. J Metamorphic Geol 22:207–226

Cherniak DJ (2010) Diffusion in accessory minerals: zircon, titanite, apatite, monazite and xenotime. Rev Mineral Geochem 72:827–869

Corfu F, Hanchar JM, Hoskin PWO, Kinny P (2003) Atlas of zircon textures. In: Hanchar JM, Hoskin PWO (eds) Zircon, vol 53. Reviews in Mineralogy, 1st edn. Mineralogical Society of America, Washington DC, pp 469–500

Cottle JM, Jessup MJ, Newell DL, Horstwood MSA, Noble SR, Parrish RR, Waters DJ, Searle MP (2009a) Geochronology of granulitized eclogite from the Ama Drime Massif: implications for the tectonic evolution of the South Tibetan Himalaya. Tectonics 28(1):TC1002

Cottle JM, Searle MP, Horstwood M, Waters DJ (2009b) Midcrustal metamorphism, melting, and deformation in the Mount Everest region of Southern Tibet revealed by U(-Th)-Pb geochronology. J Geol 117(6):643–664. doi:10.1086/605994

Dasgupta S, Ganguly J, Neogi S (2004) Crystallization history, P-T gradient, and implications. J Metamorphic Geol 22:395–412. doi:10.1111/j.1525-1314.2004.00522.x

Dasgupta S, Chakraborty S, Neogi S (2009) Petrology of an inverted Barrovian sequence of metapelites in Sikkim Himalaya, India: constraints on the tectonic inversion. Am J Sci 309:43–84. doi:10.2475/01.2009.02

Eggins SM, Rudnick RL, McDonough WF (1998) The composition of peridotites and their minerals: a laser ablation ICP-MS study. Earth Planet Sci Lett 154:53–71

Faak K, Chakraborty S, Dasgupta S (2012) Petrology and tectonic significance of metabasic slivers in the lesser- and higher Himalayan sections of Sikkim, India. J Metamorphic Geol (in press)

Faccenda M, Gerya TV, Chakraborty S (2008) Styles of post-subduction collisional orogeny: influence of convergence velocity, crustal rheology and radiogenic heat production. Lithos 103(1–2):257–287

Fletcher IR, McNaughton NJ, Davis WJ, Rasmussen B (2010) Matrix effects and calibration limitations in ion probe U-Pb and Th–Pb dating of monazite. Chem Geol 270:31–44

Foster G, Kinny P, Vance D, Prince C, Harris N (2000) The significance of monazite U-Th-Pb age data in metamorphic assemblages; a combined study of monazite and garnet chronometry. Earth Planet Sci Lett 181(3):327–340

Foster G, Gibson HD, Parrish RR, Horstwood M, Fraser J, Tindle A (2002) Textural, chemical and isotopic insight into the nature and behaviour of metamorphic monazite. Chem Geol 191(1–3): 183–207

Ganguly J, Dasgupta S, Cheng W, Neogi S (2000) Exhumation history of a section of the Sikkim Himalayas, India: records in the metamorphic mineral equilibria and compositional zoning of garnet. Earth Planet Sci Lett 183:471–486

Ghosh A (1956) Recent advances in the geology and structure of the eastern Himalaya. Indian Sci Congr 44:85–99

Godin L, Parrish RR, Brown RL, Hodges KV (2001) Crustal thickening leading to exhumation of the Himalayan metamorphic core of Central Nepal: insight from U-Pb geochronology and 40Ar/39Ar thermochronology. Tectonics 20(5):729–747

Godin L, Grujic D, Law RD, Searle MP (2006) Channel flow, ductile extrusion and exhumation in continental collision zones: an introduction. In: Law RD, Searle MP, Godin L (eds) Channel flow, ductile extrusion and exhumation in continental collision zones, vol 268. Geological Society, London, Special Publications, pp 1–23

Groppo C, Rubatto D, Rolfo F, Lombardo B (2010) Early Oligocene partial melting in the main central thrust zone (Arun Valley, Eastern Nepal, Himalaya). Lithos 118:287–301

Grujic D, Warren CJ, Wooden JL (2011) Rapid synconvergent exhumation of Miocene-aged lower orogenic crust in the eastern Himalaya. Lithosphere 3(5):346–366

Harris NBW, Caddick M, Kosler J, Goswami S, Vance D, Tindle AG (2004) The pressure-temperature-time path of migmatites from the Sikkim Himalaya. J Metamorphic Geol 22(3):249–264

Harrison TM, Ryerson FJ, Le Fort P, Yin A, Lovera OM, Catlos EJ (1997) A late miocene-pliocene origin for the Central Himalayan inverted metamorphism. Earth Planet Sci Lett 146(1–2):E1–E7

Hermann J, Rubatto D (2003) Relating zircon and monazite domains to garnet growth zones: age and duration of granulite facies metamorphism in the Val Malenco lower crust. J Metamorphic Geol 21:833–852

Hermann J, Rubatto D, Trommsdorff V (2006) Sub-solidus oligocene zircon formation in garnet peridotite during fast decompression and fluid infiltration (Duria, Central Alps). Mineral Petrol 88:181–206

Holland TJB, Powell R (2001) Calculation of phase relations involving haplogranitic melts using an internally consistent thermodynamic dataset. J Petrol 42:673–683

Hoskin PWO, Black LP (2000) Metamorphic zircon formation by solid-state recrystallization of protolith igneous zircon. J Metamorphic Geol 18:423–439

Imayama T, Takeshita T, Yi K, Cho D-L, Kitajima K, Tsutsumi Y, Kayama M, Nishido H, Okumura T, Yagi K, Itaya T, Sano Y (2012) Two-stage partial melting and contrasting cooling history within the Higher Himalayan Crystalline Sequence in the far-eastern Nepal Himalaya. Lithos 134:1–22. doi:10.1016/j.lithos.2011.12.004

Jamieson RA, Beaumont C, Medvedev S, Nguyen MH (2004) Crustal channel flows: 2. Numerical models with implications for metamorphism in the Himalayan-Tibetan orogen. J Geophys Res B: Solid Earth 109:B06407:1–B06407:24. doi:10.1029/2003JB002811

Janots E, Engi M, Berger A, Allaz J, Schwarz JO, Spandler C (2008) Prograde metamorphic sequence of REE minerals in pelitic rocks of the Central Alps: implications for allanite-monazite-xenotime phase relations from 250 to 610∞C. J Metamorphic Geol 26(5):509–526

Jessup MJ, Cottle JM, Searle MP, Law RD, Newell DL, Tracy RJ, Waters DJ (2008) P-T-t-D paths of Everest series schist, Nepal. J Metamorphic Geol 26(7):717–740

Kellett DA, Grujic D, Warren C, Cottle J, Jamieson R, Tenzin T (2010) Metamorphic history of a syn-convergent orogen-parallel detachment: the South Tibet detachment, Buthan Himalaya. J Metamorphic Geol 28(8):785–808. doi:10.1111/j.1525-1314.2010.00893.x

Kelsey DE, Clark C, Hand M (2008) Thermobarometric modelling of zircon and monazite growth in melt-bearing systems: examples using model metapelitic and metapsammitic granulites. J Metamorphic Geol 26(2):199–212

Kohn MJ, Corrie SL (2012) Preserved Zr-temperatures and U–Pb ages in high-grade metamorphic titanite: evidence for a static hot channel in the Himalayan orogen. Earth Planet Sci Lett (in press)

Kohn MJ, Wieland MS, Parkinson CD, Upreti BN (2005) Five generations of monazite in Langtang gneisses: implications for chronology of the Himalayan metamorphic core. J Metamorphic Geol 23:399–406. doi:10.1111/j.1525-1314.2005.00584.x

Kretz R (1983) Symbols for rock-forming minerals. Am Mineral 68:277–279

Lal RK, Mukherji S, Ackermand D (1981) Deformation and Barrovian metamorphismat Takdah, Darjeeling (eastern Sikkim). In: Saklani PS (ed) Metamorphic tectonics of the Himalaya. Today and Tomorrow Publishers, Delhi, pp 231–278

Liu R, Zhou H, Zhang L, Zhong Z, Zeng W, Xiang H, Jin S, Lu X, Li C (2010) Zircon U-Pb ages and Hf isotope compositions of the Mayuan migmatite complex, NW Fujian Province, Southeast China: constraints on the timing and nature of a regional tectonothermal event associated with the Caledonian orogeny. Lithos 119(3–4):163–180

Ludwig KR (2003) Isoplot/Ex version 3.0. A geochronological toolkit for Microsoft Excel. Berkeley Geochronological Centre Spec. Pub., Berkeley

Martin AJ, Gehrels GE, DeCelles PG (2007) The tectonic significance of (U, Th)/Pb ages of monazite inclusions in garnet from the Himalaya of central Nepal. Chem Geol 244:1–24

Martin AJ, Ganguly J, DeCelles PG (2010) Metamorphism of greater and lesser himalayan rocks exposed in the Modi Khola valley, central Nepal. Contrib Mineral Petrol 159(2):203–223

McDonough WF, Sun S (1995) The composition of the earth. Chem Geol 120:223–253

Oliver NHS, Bodorkos S, Nemchin AA, Kinny PD, Watt GR (1999) Relationships between zircon U-Pb SHRIMP ages and

leucosome type in migmatites of the Halls Creek Orogen, Western Australia. J Petrol 40(10):1553–1575
Pyle JM, Spear FS (2003) Four generations of accessory-phase growth in low-pressure migmatites from SW New Hampshire. Am Mineral 88(2–3):338–351
Ray SK (2000) Culmination zones in eastern Himalaya. Geological Survey of India Special publication, vol 55
Rubatto D (2002) Zircon trace element geochemistry: distribution coefficients and the link between U-Pb ages and metamorphism. Chem Geol 184:123–138
Rubatto D, Gebauer D (2000) Use of cathodoluminescence for U-Pb zircon dating by ion microprobe: some examples from the Western Alps. In: Pagel M, Barbin V, Blanc P, Ohnenstetter D (eds) Cathodoluminescence in geosciences. Springer, Berlin, pp 373–400
Rubatto D, Williams IS, Buick IS (2001) Zircon and monazite response to prograde metamorphism in the Reynolds Range, central Australia. Contrib Mineral Petrol 140:458–468
Rubatto D, Hermann J, Buick IS (2006) Temperature and bulk composition control on the growth of monazite and zircon during low-pressure anatexis (Mount Stafford, central Australia). J Petrol 47(10):1973–1996
Rubatto D, Müntener O, Barnhorn A, Gregory C (2008) Dissolution-reprecipitation of zircon at low-temperature, high-pressure conditions (Lanzo Massif, Italy). Am Mineral 93:1519–1529
Rubatto D, Hermann J, Berger A, Engi M (2009) Protracted fluid-induced melting during Barrovian metamorphism in the Central Alps. Contrib Mineral Petrol 158:703–722. doi:10.1007/s00410-009-0406-5
Schaltegger U, Fanning M, Günther D, Maurin JC, Schulmann K, Gebauer D (1999) Growth, annealing and recrystallization of zircon and preservation of monazite in high-grade metamorphism: conventional and in situ U-Pb isotope, cathodoluminescence and microchemical evidence. Contrib Mineral Petrol 134:186–201
Schärer U (1984) The effect of initial ^{230}Th disequilibrium on young U-Pb ages: the Makalu case, Himalaya. Earth Planet Sci Lett 67:191–204
Simpson RL, Parrish RR, Searle MP, Waters DJ (2000) Two episodes of monazite crystallization during metamorphism and crustal melting in the Everest region of the Nepalese Himalaya. Geology 28(5):403–406
Spear FS (2010) Monazite–allanite phase relations in metapelites. Chem Geol 279:55–62
Spear FS, Pyle JM (2002) Apatite, monazite, and xenotime in Metamorphic Rocks. In: Kohn MJ, Rakovan J, Hughes JM (eds) Phosphates: geochemical, geobiological, and materials importance vol 48. Reviews in Mineralogy and Geochemistry Mineralogical Society of America, Washington DC, pp 293–335
Spear FS, Kohn MJ, Cheney JT (1999) P–T paths from anatectic pelites. Contrib Mineral Petrol 134:17–32
Stacey JS, Kramers JD (1975) Approximation of terrestrial lead evolution by a two-stage model. Earth Planet Sci Lett 26:207–221
Stepanov AS, Hermann J, Rubatto D, Rapp RP (2012) Experimental study of monazite/melt partitioning with implications for the REE, Th and U geochemistry of crustal rocks. Chem Geol 300–301:200–220
Tomaschek F, Kennedy AK, Villa IM, Lagos M, Ballhaus C (2003) Zircons from Syros, Cyclades, Greece—recrystallization and mobilization of zircon during high-pressure metamorphism. J Petrol 44:1977–2002
Townsend KJ, Miller CF, D'Andrea JL, Ayers JC, Harrison TM, Coath CD (2000) Low temperature replacement of monazite in the Ireteba granite, Southern Nevada: geochronological implications. Chem Geol 172:95–112
Vance D, Harris N (1999) Timing of prograde metamorphism in the Zanskar Himalaya. Geology 27(5):395–398
Vavra G, Schmidt R, Gebauer D (1999) Internal morphology, habit and U-Th-Pb microanalysis of amphibolite-to-granulite facies zircons: geochronology of the Ivrea Zone (Southern Alps). Contrib Mineral Petrol 134:380–404
Viskupic K, Hodges KV, Bowring SA (2005) Timescales of melt generation and the thermal evolution of the Himalayan metamorphic core, Everest region, eastern Nepal. Contrib Mineral Petrol 149(1):1–21
Warren C, Grujic D, Kellett DA, Cottle J, Jamieson R, Ghalley KS (2011) Probing the depth of the Indian-Asia collision: U-Th-Pb monazite chronology of granulites from NW Buthan. Tectonics 30:1–24. doi:10.1029/2010TC002738
Watson EB, Wark DA, Thomas JB (2006) Crystallization thermometers for zircon and rutile. Contrib Mineral Petrol 151:413–433
White RW, Powell R, Clarke GL (2003) Prograde metamorphic assemblage evolution during partial melting of metasedimentary rocks at low pressures: migmatites from Mt Stafford, Central Australia. J Metamorphic Geol 44(11):1937–1960
Williams IS (1998) U-Th-Pb geochronology by ion microprobe. In: McKibben MA, Shanks III WC, Ridley WI (eds) Application of microanalytical techniques to understanding mineralizing processes, vol 7. Reviews in Economic Geology, Society of Economic Geologists, pp 1–35
Williams IS (2001) Response of detrital zircon and monazite, and their U-Pb isotopic systems, to regional metamorphism and host-rock partial melting, Cooma Complex, southeastern Australia. Aust J Earth Sci 48:557–580
Williams ML, Jercinovic MJ, Harlov DE, Budzyn B, Hetherington CJ (2011) Resetting monazite ages during fluid-related alteration. Chem Geol 283:218–225
Wing BN, Ferry JM, Harrison TM (2003) Prograde destruction and formation of monazite and allanite during contact and regional metamorphism of pelites: petrology and geochronology. Contrib Mineral Petrol 145(2):228–250